Numerical Modelling of Eulerian Two-Phase Gas-Solid Flow

Justin Hudson *   David Harris†

Abstract

This paper investigates the numerical solution of the equations governing two-phase flow of a solid granular material dispersed in a gas. We consider two different models in both of which the dispersed and continuous phases are treated as continua. An Eulerian description of the flow is adopted. Four different formulations of the two models are derived and a high resolution scheme is presented to obtain numerical solutions of the equations in each of the formulations. We investigate whether the chosen numerical scheme is suitable for the equations governing the models and use the numerical results to obtain quantitative and qualitative insight into the predictions of each of the models. Three test cases, new to the literature, are considered, and the numerical results compared.

1 Introduction

Many industrial and engineering processes involve the flow of several intermingled phases (solid, liquid and gaseous) and/or chemical species. In particular, chemical engineers have been much involved with the development of models of multi-phase flow and their application. For example, flow in hoppers and risers, the separation and mixing of chemicals, various processes that occur in nuclear reactors and coal combustion are just a few of the areas where chemical engineering research into multi-phase systems plays an important

*School of Mathematics, University of Manchester, Sackville Street, Manchester, M60 1QD (justin.hudson@manchester.ac.uk)

†School of Mathematics, University of Manchester, Sackville Street, Manchester, M60 1QD (david.harris@manchester.ac.uk)

role in industry. For many industrial applications it is crucial to both model the process realistically and to obtain accurate approximations to the solutions of initial and boundary value problems arising from the process and the model, in order that the process runs efficiently, that costs are reduced and that plant and process are able to operate safely. The special case of two-phase flow is the most well developed theoretically and has numerous practical applications that are crucial to industry and which may involve any combination such as liquid-gas, gas-gas etc. In this paper we are concerned with one particular combination, namely a gas-solid two phase system in which the solid phase is a granular material (by which is meant that the solid phase material is finely sub-divided into small separate grains in such a way that the volume of each grain is small in comparison to the total volume of solid) which has been dispersed in a gaseous phase. We shall refer to the gas as the continuous phase, the solid as the dispersed phase. Once dispersed the system will only remain so, at least in a terrestrial environment, if energy is continually input into the system to maintain the dispersion. This is effectively done by ensuring that the gas always *flows* and then momentum is consequently transferred from the gaseous to the solids phase by their mechanical interaction.

With regard to the flow of granular materials there are three different approaches that are commonly made to their modelling, discrete methods (for example, using particle or rigid body dynamics), statistical mechanics (which generalises the theory of dense gases to include the inelastic collisions between grains) and continuum mechanics (where both solid and fluid mechanics are applicable to granular materials, depending upon the deformation or flow regime). Two points here are worthy of mention. Firstly, for the gas-solid systems of the type considered here, the methods of fluid mechanics are appropriate, the dispersed solids phase being modelled, effectively, as a type of fluid. Secondly, a hallmark of multiphase flow is the use of hybrid models that utilise two or more of the above approaches. For example, while the gas phase is modelled as a continuum, there are essentially two ways of incorporating the solids phase into the model, namely, a discrete (Lagrangian) or continuum (Eulerian) approach. The Lagrangian method models, and keeps track of, each particle individually, whilst the Eulerian method treats averaged bulk properties of the solids phase in terms of an equivalent fluid flow. In either case, the system of equations are sufficiently complicated to prevent analytical solutions being found in all but the most trivial cases and recourse must be had to numerical methods to obtain approximations to solutions of the equations. However, due to the complexity of the models, this also is a non-trivial task and the solution of problems of relevance to industry required the advent of adequate computing power. As computing power increases it is to be expected that numerical approximations to more and more complex problems of interest to industry will become feasible and the present paper is intended as a significant contribution towards this process by analysing methods of numerical approximation in the context of models which, on the one hand are sufficiently simple to enable progress to be made on their numerical analysis and on the other hand form a sufficiently adequate basis for this type of two-phase flow.

We consider an Eulerian formulation of two-phase gas-solid flow in which both phases are treated as a continuum. The basic balance equations governing the model were established in the 1960s (see Jackson [15]). However, the constitutive equations are still in a state of development and this is an active area of research. We will not go further here into this aspect of the problem, although one paper and book of particular interest that we may cite is Jackson [16, 17]. There is an extensive literature devoted to two-phase flow in the context of problems arising in chemical engineering and an excellent introduction to the subject is provided by the monograph by Gidaspow [10].

In the early 1980's there was a significant development in the mechanics of granular materials by J.T. Jenkins and co-workers when an extension to the Kinetic Theory of dense gases to include granular materials was effected by taking into account the energy loss during collisions. There is an extensive literature, see, for example, Jenkins & Savage [18], Savage & Jeffrey [29] and Lun *et al.* [23]. One very interesting development in the chemical engineering context has been the application of this theory by its inclusion in models of gas-solid two-phase flow. The advantage of using the kinetic theory is that it enables certain material properties associated with the dispersed phase which are difficult to measure experimentally, for example the solids phase viscosity, to be calculated from the theory. Use of the kinetic theory of granular flow, however, introduces a new mechanical quantity, usually called, somewhat confusingly and inappropriately, the granular temperature, together with an energy equation containing this new quantity. It must be understood that although the name granular temperature is used in analogy with the usual word temperature, it is a mechanical quantity and not a thermodynamic quantity and is nothing to do with heat content. A major purpose of the present paper is to investigate numerically the granular temperature equation.

Another major purpose is that even though there has been a thorough investigation into Eulerian two-phase flow, modern numerical techniques have yet to be applied to such models. For example, high resolution schemes increase the accuracy of the results but can be difficult to implement into certain models, especially if the equations are inhomogeneous, as they are for two-phase flow. Thus, we analyse here two models that are well documented in the literature and obtain numerical solutions by implementing a high resolution scheme. The models are sometimes referred to in the literature as Model A and Model B. Model A originates with the work of Jackson [15], and for further details, see also Ding & Gidaspow [4] and Boemer *et al.* [2]. Model A has been stated to be ill-posed, see Lyczkowski *et al.* [25] and Stewart & Wendroff [30], due to the physical wave speeds being complex. Model B was developed by Rudinger & Chang [28], which is extended by Lyczkowski [24] (see also Gidaspow [10] and Boemer *et al.* [2]). Model B is well-posed, but the model is not as physically well based as Model A and the results of the two models can differ for certain test problems, see Boemer *et al.* [2].

In the next section we present and briefly discuss the basic equations of the two models which we shall use to model two-phase gas-solid flow. In Section 4 we present four formulations of these models and in Section 5, we present a high resolution scheme discussed by Hubbard & Garcia-Navarro [12] and Hudson [14], which is based on Roe's scheme [26], to obtain numerical approximations of the different formulations. The formulations are then compared in Section 6 for a variety of test cases to determine which approach is the most accurate. Our conclusions are presented in Section 7.

2 Mathematical Formulation

In order to develop our numerical scheme we shall consider a time varying flow in one space dimension of a two-phase gas-solid mixture, the typical application here being flow in a pipe, the lateral dimension of which is small in comparison to its length. It should be noted that the grain size must also be reasonably small in comparison with the lateral dimension. We shall assume that both the continuous gas phase and the dispersed solids phase may be represented by separate interpenetrating continua at each point of space occupied by the mixture. Of course, in the real system each point in space is occupied solely by either gas or solid, but in the model, each point x possesses the attributes of both solid and fluid material. In a sense the material has been smeared out, or averaged, throughout space, but continuum models are phenomenological and no attempt is made to define or calculate the spatial averages explicitly. Having said that, the model uses some concepts from statistical mechanics, and these, of course, are based upon ensemble averages. In this sense, the model here is a hybrid of the continuum and statistical approaches.

We shall take the pipe to lie along a portion OP of the real axis and take a coordinate system Ox, with the origin O coinciding with the left hand end of the pipe, and the positive x-direction pointing towards P. At each point x of OP the following quantities are defined. Let u_g, u_s denote the Eulerian velocity components (in the x-direction) of the gas and solid phases, respectively, ρ_g, ρ_s the density of the gas and grains. In the real mixture, let V denote the volume of a representative volume (i.e. a volume containing a representative mixture of gas and grain), V_g and V_s denote the portions of this representative volume occupied by gas and grains respectively, then the gas volume fraction and solids volume fraction are defined by

$$\frac{V_g}{V} \quad \text{and} \quad \frac{V_s}{V} \tag{2.1}$$

respectively. It is a fundamental assumption of the continuum model, that there exist two functions ϵ_g and ϵ_s, which we shall call the gas and solids volume fractions, respectively and which satisfy the following properties

$$0 \leq \epsilon_g \leq 1, \qquad 0 \leq \epsilon_s \leq 1 \qquad \text{and} \qquad \epsilon_g + \epsilon_s = 1. \tag{2.2}$$

Finally, let T_s denote the so-called granular temperature of the solids phase. The physical interpretation of T_s is that it is the square of the deviation of the individual grains velocity from the mean grain velocity.

2.1 The Model Equations

The conservation laws governing the model have been derived many times in the literature, we may cite for example Jackson [16, 17]. The conservation of mass for each phase gives rise to the following pair of continuity equations and are the same for both models A and B:

$$\frac{\partial}{\partial t}(\epsilon_g \rho_g) + \frac{\partial}{\partial x}(\epsilon_g \rho_g u_g) = 0 \tag{2.3}$$

and

$$\frac{\partial}{\partial t}(\epsilon_s \rho_s) + \frac{\partial}{\partial x}(\epsilon_s \rho_s u_s) = 0. \tag{2.4}$$

On the other hand, the balance of linear momentum equations differ between models A and B. The exact form of the conservation of linear momentum depends upon the choice of constitutive equation and also upon the choice of interaction laws between the two phases. We wish to make simple but representative choices. Two commonly used forms for the interaction force between the two phases are Stokes' law, for laminar flow and moderate relative velocities which is linear in the phase velocity difference $u_g - u_s$ and Newton's law, for turbulent flow and which is quadratic in $u_g - u_s$. The precise form that we shall use is given by the expression

$$\beta = \frac{C_D}{d_s} \epsilon_g \epsilon_s \rho_g (u_g - u_s), \tag{2.5}$$

where C_D is a dimensionless parameter. Thus, viscosity is taken into account via the interphase drag force. However, we shall omit viscosity from the constitutive equation and assume the gas phase to behave as an inviscid, compressible fluid obeying the perfect gas law

$$p_g(\rho_g) = C_p \rho_g^{\gamma}. \tag{2.6}$$

Thus the stress tensor is diagonal and the balance of linear momentum for the gas phase for model A may be written

$$\frac{\partial}{\partial t}(\epsilon_g \rho_g u_g) + \frac{\partial}{\partial x}(\epsilon_g \rho_g u_g^2) + \epsilon_g \frac{\partial p_g}{\partial x} = -\beta(u_g - u_s) \tag{2.7}$$

while the balance of linear momentum for the solids phase for model A may be written

$$\frac{\partial}{\partial t}(\epsilon_s \rho_s u_s) + \frac{\partial}{\partial x}(\epsilon_s \rho_s u_s^2 + p_s) + \epsilon_s \frac{\partial p_g}{\partial x} = \beta(u_g - u_s). \tag{2.8}$$

where, in this paper, for both models, the solids pressure is assumed to satisfy the following law, which is analogous to the perfect gas law,

$$p_s(\epsilon_s, T_s) = \epsilon_s \rho_s T_s \tag{2.9}$$

It should be emphasised that this law is the simplest one possible and we choose it so we may clearly illustrate the numerical techniques used to approximate both models. It is, effectively, the first term of an expression for the solids pressure p_s obtained from the kinetic theory of granular materials. A more accurate law would incorporate both energy dissipation and also a non-trivial radial distribution function. It should be noted that the numerical techniques discussed in this paper may be modified to include this extra term and work is currently in progress to do this.

For model B the linear momentum equations are

$$\frac{\partial}{\partial t}(\epsilon_g \rho_g u_g) + \frac{\partial}{\partial x}(\epsilon_g \rho_g u_g^2 + p_g) = -\beta(u_g - u_s) \tag{2.10}$$

and

$$\frac{\partial}{\partial t}\epsilon_s \rho_s u_s) + \frac{\partial}{\partial x}(\epsilon_s \rho_s u_s^2 + p_s) = \beta(u_g - u_s) \tag{2.11}$$

for the gas and solids phases, respectively. Finally, the granular temperature equation, which is an energy equation, is

$$\frac{\partial}{\partial t}(\epsilon_s \rho_s T_s) + \frac{\partial}{\partial x}(\epsilon_s \rho_s u_s T_s) = -\frac{2}{3}\left(p_s \frac{\partial u_s}{\partial x} + 3\beta T_s\right) \tag{2.12}$$

We shall take the solids density ρ_s to be a constant. This is both an accurate approximation and the simplest way to close the models. Note that, however, the gas density ρ_g is not assumed to be constant. The governing equations for both models are conveniently summarised in Table 2.1, where a subscript $k = g$ ($k = s$) denotes the gas phase (solids phase). Also, the physical quantities appearing in the models are summarised in Table 2.2.

Mass (A and B)	$(\epsilon_k \rho_k)_t + (\epsilon_k \rho_k u_k)_x = 0$
Momentum (A gas)	$(\epsilon_g \rho_g u_g)_t + (\epsilon_g \rho_g u_g^2)_x + \epsilon_g (p_g)_x = -\beta_A (u_g - u_s)$
Momentum (A solid)	$(\epsilon_s \rho_s u_s)_t + (\epsilon_s \rho_s u_s^2 + p_s)_x + \epsilon_s (p_g)_x = \beta (u_g - u_s)$
Momentum (B gas)	$(\epsilon_g \rho_g u_g)_t + (\epsilon_g \rho_g u_g^2 + p_g)_x = -\beta (u_g - u_s)$
Momentum (B solid)	$(\epsilon_s \rho_s u_s)_t + (\epsilon_s \rho_s u_s^2 + p_s)_x = \beta (u_g - u_s)$
Granular Temperature (A and B)	$(\epsilon_s \rho_s T_s)_t + (\epsilon_s \rho_s u_s T_s)_x = -\frac{2}{3}\left(p_s (u_s)_x + 3\beta T_s\right)$
Gas Pressure	$p_g(\rho_g) = C_p \rho_g^\gamma$
Solids Pressure	$p_s(\epsilon_s, T_s) = \epsilon_s \rho_s T_s$
Drag Force	$\beta = \frac{C_D}{d_s} \epsilon_g \epsilon_s \rho_g (u_g - u_s)$
Gas Phase Sound Speed	$c_g = \sqrt{\frac{\partial p_g}{\partial \rho_g}} = \sqrt{C_p \gamma \rho_g^{\gamma - 1}}$
Solids Phase Propagation Velocity	$c_s = \sqrt{\frac{\partial p_s}{\partial \epsilon_s}} = \sqrt{\rho_s T_s}$
Sum of Volume Fractions	$\epsilon_g + \epsilon_s = 1$

Table 2.1: Summary of Equations for Models A and B

Name	Symbol	Units
Density	$\rho_k(x,t)$	$\mathrm{kg/m^3}$
Velocity	$u_k(x,t)$	$\mathrm{m/s}$
Temperature	$T_s(x,t)$	$\mathrm{m^2/s^2}$
Volume Fraction	$\epsilon_k(x,t)$	none
Gravity	g	$\mathrm{m/s^2}$
Gas Pressure	$p_g(\rho_g)$	$\mathrm{kg/(ms^2)}$
Solids Pressure	$p_s(\epsilon_s, T_s)$	$\mathrm{kg/(ms^2)}$
Drag Force	β	$\mathrm{kg/(m^3s)}$
Solids Particle Diameter	d_s	m

Table 2.2: Physical Quantities Occurring in Models A and B

2.2 Gas and Solids Data

We consider the case of glass beads being transported by air and take a solids density of $\rho_s = 2660$ kg/m^3 and particle diameter $d_s = 0.005$ m. For the gas phase, data corresponding to air at room temperature (20°C) with atmospheric pressure (100.0437 kPa), density $\rho_g = 1.2885$ kg/m^3 and viscosity $\mu_g = 1.58 \times 10^{-7}$ Pa.s are taken. Also $\gamma_g = 1.4$ and $C_p = 75916.16$ m$^{3.2}$/(kg$^{0.4}$s^2).

Since the gas flow is at moderate velocities and room temperature it is physically appropriate to assume an isentropic gas flow. Thus, shocks in the gas phase are not permissible. However, two-phase flows have a richer shock structure than single-phase and there are shocks involving the solids phase which, for the gas phase only involve discontinuities in ϵ_g and u_g, while ρ_g remains continuous. Such shocks do not violate the assumption of constant entropy. Perturbations in the gas phase evolve on a considerably faster time scale than those of the solids phase, since $|\lambda_g| \gg |\lambda_s|$, so shocks due to the solids phase propagate slowly in comparison with the gas speed of sound.

3 Hyperbolicity

In this section we consider whether each model is hyperbolic for the regime under investigation, both for the suitability of the scheme and for the implementation of the initial and boundary conditions for the test cases. We intend to solve the equations only in regimes where the equations are hyperbolic and need to investigate when this is the case.

A system of partial differential equations is hyperbolic if the physical wave speeds (obtained from the canonical form) of the system are all real and there exists a complete set of linearly independent eigenvectors, see LeVeque [21]. A full set of linearly independent eigenvectors can be found for both models thus, we must ensure that the wave speeds are all real.

3.1 Model A

We can rewrite the system of equations for Model A in canonical form

$$\begin{bmatrix} \rho_g \\ u_g \\ \epsilon_s \\ u_s \\ T_s \end{bmatrix}_t + \begin{bmatrix} u_g & \rho_g & \frac{\rho_g}{\epsilon_g}(u_s - u_g) & \frac{\rho_g \epsilon_s}{\epsilon_g} & 0 \\ \frac{c_g^2}{\rho_g} & u_g & 0 & 0 & 0 \\ 0 & 0 & u_s & \epsilon_s & 0 \\ \frac{c_g^2}{\rho_s} & 0 & \frac{T_s}{\epsilon_s} & u_s & 1 \\ 0 & 0 & 0 & \frac{2}{3}T_s & u_s \end{bmatrix} \begin{bmatrix} \rho_g \\ u_g \\ \epsilon_s \\ u_s \\ T_s \end{bmatrix}_x = \begin{bmatrix} 0 \\ -\frac{\beta}{\epsilon_g \rho_g}(u_g - u_s) \\ 0 \\ \frac{\beta}{\rho_s \epsilon_s}(u_g - u_s) \\ -\frac{2\beta T_s}{\rho_s \epsilon_s} \end{bmatrix},$$

where

$$c_g^2 = \frac{\partial p_g}{\partial \rho_g} = C_p \gamma_g \rho_g^{\gamma_g - 1}.$$

For this system, the characteristic equation is

$$(\lambda - u_s)Q(\lambda) = 0,$$

where $Q(\lambda)$ is the quartic,

$$Q(\lambda) = a_4\lambda^4 + a_3\lambda^3 + a_2\lambda^2 + a_1\lambda + a_0,$$

whose components are

$$a_4 = 3\rho_s\epsilon_g, \quad a_3 = -6\rho_s\epsilon_g(u_g + u_s),$$

$$a_2 = -3c_g^2(\epsilon_g\rho_s + \epsilon_s\rho_g) - 5\rho_s\epsilon_g T_s + 3\rho_s\epsilon_g(u_s^2 + u_g^2 + 4u_g u_s),$$

$$a_1 = 6c_g^2(\epsilon_g\rho_s u_s + \epsilon_s\rho_g u_g) + 10\rho_s\epsilon_g u_g T_s - 6\rho_s\epsilon_g u_g u_s(u_s + u_g)$$

and

$$a_0 = -3c_g^2(\epsilon_g\rho_s u_s^2 + \epsilon_s\rho_g u_g^2) + 3\rho_s\epsilon_g u_g^2 u_s^2 + 5\rho_s T_s\epsilon_g(c_g^2 - u_g^2).$$

Thus, one root is always real and the other four are determined by solving the quartic. The roots of the quartic for the model in general have not been found analytically. Thus, we use Matlab to determine the roots numerically. We use the constant values in Section 2.2 and then solve the quartic for a variety of values of the remaining variables appearing in the coefficients a_k. The Matlab program calculates the values of a_k, calculates the roots numerically using the built in command c=roots(a_k) and determines if any root is complex by using the command image(c), with image(c)$\neq 0$ if a root is complex.

Figures 3.1 and 3.2 illustrate various contour plots for certain fixed values of ϵ_s, ρ_g and T_s to show combinations of values resulting in complex roots. The coefficients of the quartic may readily be re-written in terms of $u_g - u_s$ and $u_g + u_s$ and from Figure 3.1, we can

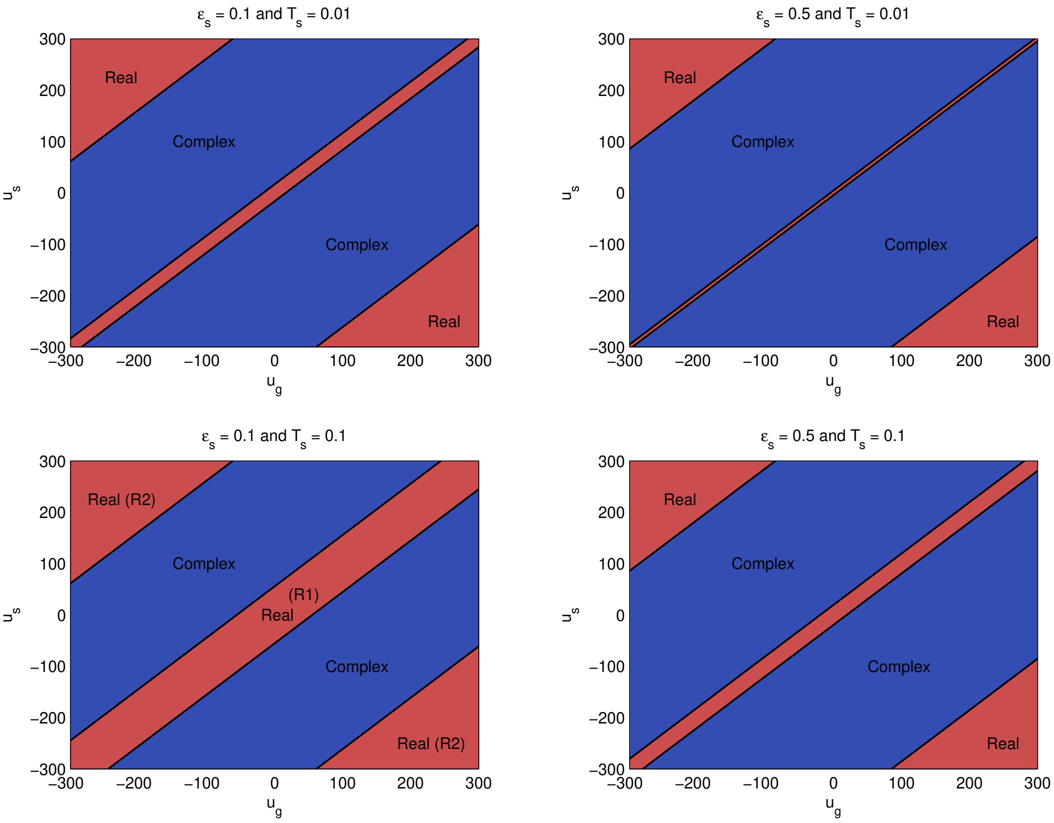

Figure 3.1: Hyperbolicity of Model A for different velocities.

see that $u_g - u_s$ plays an important role. The graph shows two regions of real roots, both dependent on $u_g - u_s$. The region of real roots for small relative velocities (R1) increases in width as T_s is increased whereas the real region of real roots for large relative velocities (R2) is slightly reduced. Moreover, as ϵ_s is increased, both regions R1 and R2 decrease in width. Changing the gas density also has an impact on the region of real roots and reduces the width of both regions R1 and R2. This behaviour is verified by Figure 3.2. Thus, Model A is hyperbolic for a restricted set of values of the quantities appearing in the coefficients.

The results show that fixed values of $u_g - u_s = C$, where C is a constant, produces identical regions of real roots, regardless of the individual values of u_g and u_s. Setting one velocity equal to zero simplifies the analysis and Figure 3.3 illustrates the graph of the quartic for different relative velocities with one of the velocities equal to zero. From the results, we can see that the real region R1 is created by a maximum, which appears at $\lambda \approx u_s$, and is destroyed when the value of the quartic is less than zero for the position of this maximum,

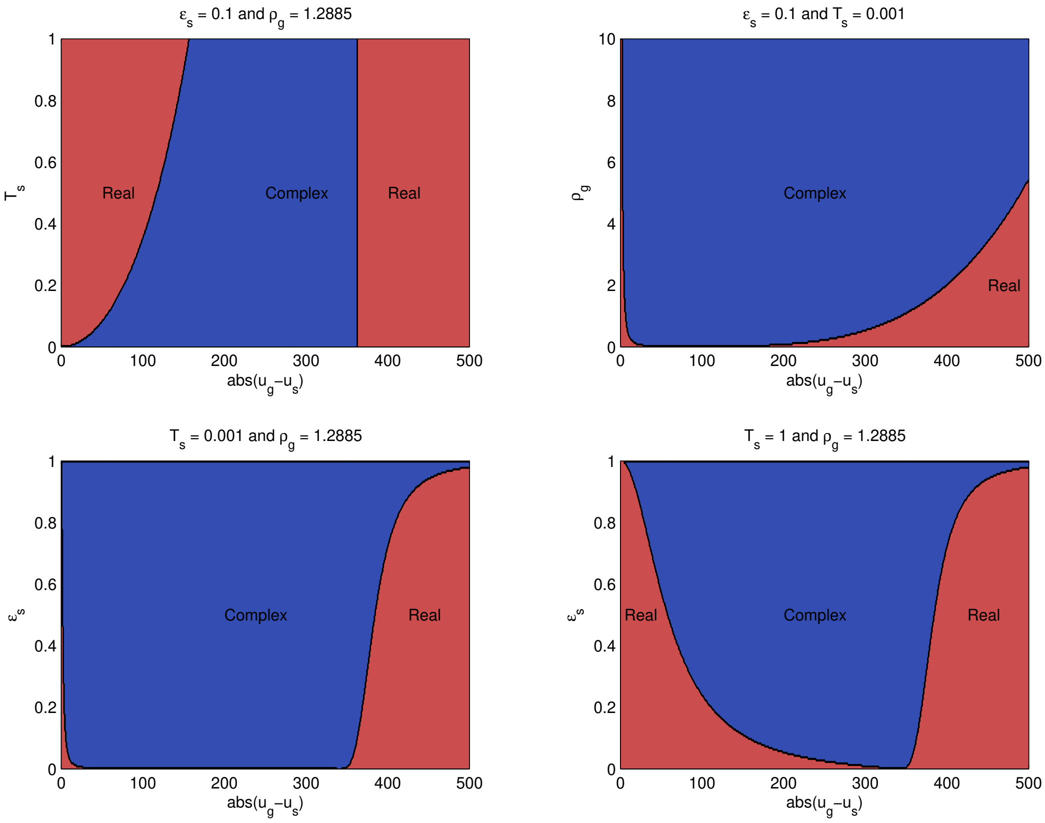

Figure 3.2: Hyperbolicity of Model A for $u_g = 0$

i.e. $Q(u_s) < 0$. By letting $u_s = 0$, we see the maximum remains approximately at the origin for small relative velocities. Thus, by assuming the position of the maximum is at $\lambda = u_s$ and by letting $u_s = 0$, we obtain the following inequality

$$-3c_g^2\epsilon_s\rho_g u_g^2 + 5\rho_s T_s \epsilon_g (c_g^2 - u_g^2) > 0,$$

which determines whether or not the region of real roots R1 exists. A similar inequality in terms of u_s can be obtained by setting $u_g = 0$. Thus, since the region of real roots is unaltered for the same relative velocities, we obtain a more general inequality

$$(u_g - u_s)^2 < \frac{5\rho_s T_s \epsilon_g c_g^2}{3c_g^2\epsilon_s\rho_g + 5\rho_s T_s \epsilon_g}$$

to determine the maximum value of relative velocities allowed for the real region R1. When compared to the position of the maximum computed by Matlab using $Q(\lambda) = 0$, in every run performed the inequality gave a good indication of the true value, and, in every case, correctly predicted the existence of real roots.

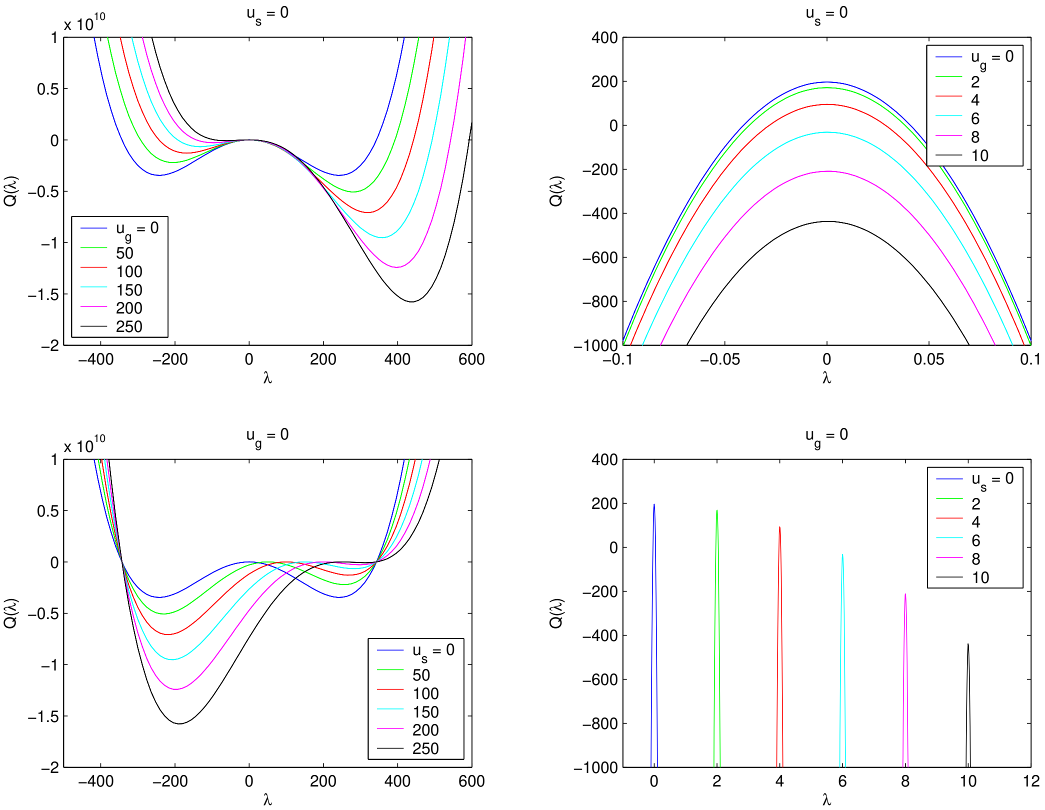

Figure 3.3: Analysis of the quartic for Model A with $T_s = 0.001$, $\rho_g = 1.2885$ and $\epsilon_s = 0.1$.

In conclusion, for Model A there exists a small region of real roots when the relative velocity is sufficiently small. It is known that the original model of Jackson [15] for inviscid flow, i.e. $p_s = 0$, is not hyperbolic for small relative velocities, see Lyczkowski *et al.* [25], Drew [5] and Stewart & Wendroff [30]. However, by including the solids pressure term in the solids phase, a new region of real roots for small relative velocities is created. Moreover, for the model presented here, $p_s = 0$ only if either $\epsilon_s = 0$ or $T_s = 0$. If there is a region of pure gas, i.e. $\epsilon_s = 0$, the quartic has four real roots. When $T_s = 0$, two of the roots of the quartic are complex for small relative velocities, but the model is not valid in this limit, since then there are no velocity fluctuations and hence no collisions between grains.

3.2 Model B

We can rewrite the system of equations for Model B in canonical form

$$\begin{bmatrix} \rho_g \\ u_g \\ \epsilon_s \\ u_s \\ T_s \end{bmatrix}_t + \begin{bmatrix} u_g & \rho_g & \frac{\rho_g}{\epsilon_g}(u_s - u_g) & \frac{\rho_g \epsilon_s}{\epsilon_g} & 0 \\ \frac{c_g^2}{\epsilon_g \rho_g} & u_g & 0 & 0 & 0 \\ 0 & 0 & u_s & \epsilon_s & 0 \\ 0 & 0 & \frac{T_s}{\epsilon_s} & u_s & 1 \\ 0 & 0 & 0 & \frac{2}{3}T_s & u_s \end{bmatrix} \begin{bmatrix} \rho_g \\ u_g \\ \epsilon_s \\ u_s \\ T_s \end{bmatrix}_x = \begin{bmatrix} 0 \\ -\frac{\beta}{\epsilon_g \rho_g}(u_g - u_s) \\ 0 \\ \frac{\beta}{\rho_s \epsilon_s}(u_g - u_s) \\ -\frac{2\beta T_s}{\rho_s \epsilon_s} \end{bmatrix},$$

where

$$c_g^2 = \frac{\partial p_g}{\partial \rho_g} = C_p \gamma_g \rho_g^{\gamma_g - 1},$$

from which the wave speeds can easily be obtained,

$$\lambda_{1,2} = u_g \pm c_g \sqrt{\epsilon_g^{-1}}, \quad \lambda_3 = u_s \quad \text{and} \quad \lambda_{4,5} = u_s \pm \frac{1}{3}\sqrt{15 T_s}.$$

Hence, Model B is hyperbolic since there are 5 real and distinct eigenvalues. Moreover, two of the roots are associated with the gas-phase ($\lambda_{1,2}$) and three with the solids-phase ($\lambda_{3,4,5}$).

4 Formulations of Models A and B

In order to help maximise the accuracy of the high resolution scheme which is presented in Section 5, we present four different formulations of the models, two of which are based on Model A and the other two on Model B. Each is written in conservative variable form to ensure that shocks propagate at the correct speed and comprises a system of inhomogeneous conservation laws which may be written as

$$\mathbf{w}_t + \mathbf{F}(\mathbf{w})_x = \mathbf{R} + \mathbf{S}, \tag{4.1}$$

where $\mathbf{F}(\mathbf{w})$ denotes the flux-function, $\mathbf{R}$ denotes the inhomogeneous terms which contain spatial derivatives of the dependent variables and $\mathbf{S}$ denotes the remaining inhomogeneous terms without such derivatives. The inhomogeneous terms are split in this manner to aid the numerical discretisation presented in the next section.

4.1 Formulation AS

The first formulation of Model A gives rise to a system of equations which will be called AS and involves writing the gas pressure gradient term in the gas-phase equation of motion in an alternative way. Now, from equations (2.7), (2.8), the equations of motion for Model A contain the spatial derivative of the gas pressure multiplied by a volume fraction. From a numerical perspective, it is desirable to have the homogeneous part of the gas phase equations as similar in form as possible to the standard Euler equations. This is mainly due to the Jacobian matrix of the system, as written in equations (2.7), (2.8), possessing repeated roots, and this may cause difficulties in approximating the system. Hence, we rewrite the gas pressure term as

$$\epsilon_g(p_g)_x = (p_g)_x - \epsilon_s(p_g)_x,$$

thus obtaining

$$\begin{bmatrix} \epsilon_g\rho_g \\ \epsilon_g\rho_g u_g \\ \epsilon_s \\ \epsilon_s u_s \\ \epsilon_s T_s \end{bmatrix}_t + \begin{bmatrix} \epsilon_g\rho_g u_g \\ \epsilon_g\rho_g u_g^2 + p_g \\ \epsilon_s u_s \\ \epsilon_s u_s^2 + \epsilon_s T_s \\ \epsilon_s u_s T_s \end{bmatrix}_x = \begin{bmatrix} 0 \\ \epsilon_s(p_g)_x \\ 0 \\ -\rho_s^{-1}\epsilon_s(p_g)_x \\ -\frac{2}{3}\epsilon_s T_s(u_s)_x \end{bmatrix} + \begin{bmatrix} 0 \\ -\beta(u_g - u_s) \\ 0 \\ \rho_s^{-1}\beta(u_g - u_s) \\ -2\rho_s^{-1}\beta T_s \end{bmatrix}, \tag{4.2}$$

with Jacobian matrix

$$\mathbf{J} = \begin{bmatrix} 0 & 1 & 0 & 0 & 0 \\ \epsilon_g^{-1}c_g^2 - u_g^2 & 2u_g & \rho_g\epsilon_g^{-1}c_g^2 & 0 & 0 \\ 0 & 0 & 0 & 1 & 0 \\ 0 & 0 & -u_s^2 & 2u_s & 1 \\ 0 & 0 & -u_s T_s & T_s & u_s \end{bmatrix}.$$

4.2 Formulation AP

The second formulation of Model A gives rise to a system of equations which will be called AP, and the purpose of this reformulation is to write the work-rate term in the granular temperature equation (2.12) in an alternative way. The inhomogeneous term $-p_s(u_s)_x$ present on the right-hand side of the granular temperature equation is an important term and, thus, it may create difficulties in numerically approximating the equations. To try to resolve this difficulty, we use the product rule to re-write this term,

$$-\frac{2}{3}\epsilon_s T_s(u_s)_x = -\frac{2}{3}(\epsilon_s u_s T_s)_x + \frac{2}{3}u_s(\epsilon_s T_s)_x,$$

and include part of it in the flux-function. The purpose of this is to obtain a less significant inhomogeneous term on the right hand side. By using this approach, we obtain

$$\begin{bmatrix} \epsilon_g\rho_g \\ \epsilon_g\rho_g u_g \\ \epsilon_s \\ \epsilon_s u_s \\ \epsilon_s T_s \end{bmatrix}_t + \begin{bmatrix} \epsilon_g\rho_g u_g \\ \epsilon_g\rho_g u_g^2 + p_g \\ \epsilon_s u_s \\ \epsilon_s u_s^2 + \epsilon_s T_s \\ \frac{5}{3}\epsilon_s u_s T_s \end{bmatrix}_x = \begin{bmatrix} 0 \\ \epsilon_s (p_g)_x \\ 0 \\ -\rho_s^{-1}\epsilon_s (p_g)_x \\ \frac{2}{3}u_s(\epsilon_s T_s)_x \end{bmatrix} + \begin{bmatrix} 0 \\ -\beta(u_g - u_s) \\ 0 \\ \rho_s^{-1}\beta(u_g - u_s) \\ -2\rho_s^{-1}\beta T_s \end{bmatrix}, \tag{4.3}$$

with Jacobian matrix

$$\mathbf{J} = \begin{bmatrix} 0 & 1 & 0 & 0 & 0 \\ \epsilon_g^{-1}c_g^2 - u_g^2 & 2u_g & \rho_g\epsilon_g^{-1}c_g^2 & 0 & 0 \\ 0 & 0 & 0 & 1 & 0 \\ 0 & 0 & -u_s^2 & 2u_s & 1 \\ 0 & 0 & -\frac{5}{3}u_s T_s & \frac{5}{3}T_s & \frac{5}{3}u_s \end{bmatrix}.$$

4.3 Formulation BS

Turning now to Model B, there is no need to re-write the pressure gradient term in the gas-phase equation of motion, and the most straightforward way to formulate the model, system BS, is to write the equations (2.3), (2.4), (2.10), (2.11) and (2.12) as,

$$\begin{bmatrix} \epsilon_g\rho_g \\ \epsilon_g\rho_g u_g \\ \epsilon_s \\ \epsilon_s u_s \\ \epsilon_s T_s \end{bmatrix}_t + \begin{bmatrix} \epsilon_g\rho_g u_g \\ \epsilon_g\rho_g u_g^2 + p_g \\ \epsilon_s u_s \\ \epsilon_s u_s^2 + \epsilon_s T_s \\ \epsilon_s u_s T_s \end{bmatrix}_x = \begin{bmatrix} 0 \\ 0 \\ 0 \\ 0 \\ -\frac{2}{3}\epsilon_s T_s (u_s)_x \end{bmatrix} + \begin{bmatrix} 0 \\ -\beta(u_g - u_s) \\ 0 \\ \rho_s^{-1}\beta(u_g - u_s) \\ -2\rho_s^{-1}\beta T_s \end{bmatrix}, \tag{4.4}$$

with Jacobian matrix identical to that of Formulation AS.

4.4 Formulation BP

The second formulation for Model B gives rise to the following system of equations BP. As with system AP for Model A, we re-write the important term present in the granular temperature equation by using the product rule, thus obtaining

$$\begin{bmatrix} \epsilon_g\rho_g \\ \epsilon_g\rho_g u_g \\ \epsilon_s \\ \epsilon_s u_s \\ \epsilon_s T_s \end{bmatrix}_t + \begin{bmatrix} \epsilon_g\rho_g u_g \\ \epsilon_g\rho_g u_g^2 + p_g \\ \epsilon_s u_s \\ \epsilon_s u_s^2 + \epsilon_s T_s \\ \frac{5}{3}\epsilon_s u_s T_s \end{bmatrix}_x = \begin{bmatrix} 0 \\ 0 \\ 0 \\ 0 \\ \frac{2}{3}u_s(\epsilon_s T_s)_x \end{bmatrix} + \begin{bmatrix} 0 \\ -\beta(u_g - u_s) \\ 0 \\ \rho_s^{-1}\beta(u_g - u_s) \\ -2\rho_s^{-1}\beta T_s \end{bmatrix}, \tag{4.5}$$

with Jacobian matrix identical to that of the system AP.

We emphasise the point made above that the inhomogeneous term, $-p_s(u_s)_x$, on the right hand side of the granular temperature equation (2.12) plays an important role in both the evolution and the steady state values of the granular temperature. Moreover, this term can create difficulties for numerical schemes that do not approximate the inhomogeneous terms with sufficient accuracy. Thus, it is of great importance that the inhomogeneous terms are discretised appropriately with the understanding that they play a significant role in the solution of the equations. Notice that Model A has more inhomogeneous terms than Model B and as a consequence we may anticipate that Model A will be more difficult to numerically approximate than Model B.

Having obtained four closely related systems of equations in conservation form, in the next section we investigate how to obtain accurate numerical approximations to these systems.

5 High Resolution Scheme

We propose a numerical scheme to approximate the different system discussed in the previous section. The scheme is chosen to be second order accurate away from discontinuities and minimises the dispersion present in second order schemes by adding dissipation in the neighbourhood of a discontinuity, i.e. we choose a high resolution scheme [11]. Since the system under investigation is inhomogeneous, the high resolution scheme must be capable of successfully incorporating the inhomogeneous terms. Inhomogeneous terms are renowned for creating numerical difficulties, see for example LeVeque & Yee [22], with numerous techniques being developed to try and resolve them, see Gascon & Corberan [7], LeVeque [20] and Bermúdez & Vázquez [1].

We use a high resolution scheme discussed by Hubbard & Garcia-Navarro [12], which is based on Roe's scheme [26]. We consider two different methods of approximating the inhomogeneous terms: a pointwise method and an upwind method. The upwind method

Roe Averages		
$\tilde{u}_g = \frac{\sqrt{(\epsilon_g\rho_g)_L}(u_g)_L + \sqrt{(\epsilon_g\rho_g)_R}(u_g)_R}{\sqrt{(\epsilon_g\rho_g)_L} + \sqrt{(\epsilon_g\rho_g)_R}}$	$\tilde{\epsilon}_g = \frac{1}{2}\left((\epsilon_g)_R + (\epsilon_g)_L\right)$	$\tilde{p}_g = \frac{1}{2}\left((p_g)_R + (p_g)_L\right)$
$\tilde{T}_s = \frac{\sqrt{(\epsilon_s)_L}(T_s)_L + \sqrt{(\epsilon_s)_R}(T_s)_R}{\sqrt{(\epsilon_s)_L} + \sqrt{(\epsilon_s)_R}}$	$\tilde{\epsilon}_s = \frac{1}{2}\left((\epsilon_s)_R + (\epsilon_s)_L\right)$	$\tilde{c}_g = \begin{cases} \sqrt{\frac{\Delta p_g}{\Delta \rho_g}} & \text{if } \Delta\rho_g \neq 0 \\ c_g(\rho_g) & \text{otherwise} \end{cases}$
$\tilde{u}_s = \frac{\sqrt{(\epsilon_s)_L}(u_s)_L + \sqrt{(\epsilon_s)_R}(u_s)_R}{\sqrt{(\epsilon_s)_L} + \sqrt{(\epsilon_s)_R}}$	$\tilde{\rho}_g = \frac{1}{2}\left((\rho_g)_R + (\rho_g)_L\right)$	$\tilde{d}_k = \frac{\tilde{u}_g^2\tilde{\epsilon}_g - \tilde{c}_g^2 - (2\tilde{u}_g - \tilde{\lambda}_k)\tilde{\epsilon}_g\tilde{\lambda}_k}{\tilde{\rho}_g\tilde{c}_g^2}$
Eigenvalues		
$\tilde{\lambda}^S_{1,2} = \tilde{u}_g \mp \tilde{c}_g\sqrt{\tilde{\epsilon}_g^{-1}}, \quad \tilde{\lambda}^S_3 = \tilde{u}_s \quad \text{and} \quad \tilde{\lambda}^S_{4,5} = \tilde{u}_s \mp \sqrt{\tilde{T}_s}$		
$\tilde{\lambda}^P_{1,2} = \tilde{u}_g \mp \tilde{c}_g\sqrt{\tilde{\epsilon}_g^{-1}}, \quad \tilde{\lambda}^P_3 = \tilde{u}_s \quad \text{and} \quad \tilde{\lambda}^P_{4,5} = \frac{4}{3}\tilde{u}_s \mp \frac{1}{3}\sqrt{\tilde{u}_s^2 + 15\tilde{T}_s}$		
Eigenvectors		
$\tilde{\mathbf{e}}_{1,2} = \begin{bmatrix} 1 \\ \tilde{\lambda}_{1,2} \\ 0 \\ 0 \\ 0 \end{bmatrix}$	$\tilde{\mathbf{e}}_3 = \begin{bmatrix} 1 \\ \tilde{u}_s \\ \tilde{d}_3 \\ \tilde{u}_s\tilde{d}_3 \\ 0 \end{bmatrix}$	$\tilde{\mathbf{e}}_{4,5} = \begin{bmatrix} 1 \\ \tilde{\lambda}_{4,5} \\ \tilde{d}_{4,5} \\ \tilde{\lambda}_{4,5}\tilde{d}_{4,5} \\ (\tilde{\lambda}_{4,5} - \tilde{u}_s)^2\tilde{d}_{4,5} \end{bmatrix}$
Wave Strengths		
$\tilde{\alpha}^{3,4,5}_k = \frac{(\tilde{\lambda}_a\tilde{\lambda}_b - \tilde{u}_s^2)\Delta\epsilon_s - (\tilde{\lambda}_a + \tilde{\lambda}_b - 2\tilde{u}_s)\Delta(\epsilon_s u_s) + \Delta(\epsilon_s T_s)}{\tilde{d}_k(\tilde{\lambda}_k - \tilde{\lambda}_a)(\tilde{\lambda}_k - \tilde{\lambda}_b)} \quad \text{where} \quad a \neq k \neq b$		
$\tilde{\alpha}_{1,2} = \mp\frac{\tilde{\lambda}_3\tilde{\alpha}_3 + \tilde{\lambda}_4\tilde{\alpha}_4 + \tilde{\lambda}_5\tilde{\alpha}_5 - (\tilde{\alpha}_3 + \tilde{\alpha}_4 + \tilde{\alpha}_5 - \Delta(\epsilon_g\rho_g))\tilde{\lambda}_{2,1} - \Delta(\epsilon_g\rho_g u_g)}{\tilde{\lambda}_1 - \tilde{\lambda}_2}$		
Inhomogeneous Terms		
$\tilde{\beta}^{3,4,5}_k = \frac{(2\tilde{u}_s - \tilde{\lambda}_a - \tilde{\lambda}_b)\tilde{r}_4 + \tilde{r}_5}{\tilde{d}_k(\tilde{\lambda}_k - \tilde{\lambda}_a)(\tilde{\lambda}_k - \tilde{\lambda}_b)} \quad (k \neq a \neq b) \quad \tilde{\beta}_{1,2} = \mp\frac{\tilde{\lambda}_3\tilde{\beta}_3 + \tilde{\lambda}_4\tilde{\beta}_4 + \tilde{\lambda}_5\tilde{\beta}_5 - (\tilde{\beta}_3 + \tilde{\beta}_4 + \tilde{\beta}_5)\tilde{\lambda}_{2,1} - \tilde{r}_2}{\tilde{\lambda}_1 - \tilde{\lambda}_2}$		
Model A	$\tilde{r}_2 = \tilde{\epsilon}_s\Delta p_g, \quad \tilde{r}_4 = -\frac{\tilde{\epsilon}_s}{\rho_s}\Delta p_g, \quad \tilde{r}^S_5 = -\frac{2}{3}\tilde{\epsilon}_s\tilde{T}_s\Delta u_s \quad \text{and} \quad \tilde{r}^P_5 = \frac{2}{3}\tilde{u}_s\Delta(\epsilon_s T_s)$	
Model B	$\tilde{r}_2 = 0, \quad \tilde{r}_4 = 0, \quad \tilde{r}^S_5 = -\frac{2}{3}\tilde{\epsilon}_s\tilde{T}_s\Delta u_s \quad \text{and} \quad \tilde{r}^P_5 = \frac{2}{3}\tilde{u}_s\Delta(\epsilon_s T_s)$	

Table 5.1: Roe Average Values (superscripts denote formulation)

applies flux-limiters, see Sweby [31], to the inhomogeneous terms as well as the flux-function to ensure a balance occurs between the terms for steady state problems (known as the C-property [1], see Appendix B). Both methods have been widely used for the shallow water equations and Euler's equations with varying degrees of success. We adapt the scheme for the Eulerian gas-solid two-phase flow models considered here. The scheme consists of

$$\mathbf{w}_i^{n+1} = \mathbf{w}_i^n - s(\mathbf{F}^*_{i+\frac{1}{2}} - \mathbf{F}^*_{i-\frac{1}{2}}) + s\mathbf{R}_i^* + \Delta t \mathbf{S}_i^n, \tag{5.1}$$

with numerical flux-function

$$\mathbf{F}^*_{i+\frac{1}{2}} = \frac{1}{2}(\mathbf{F}^n_{i+1} + \mathbf{F}^n_i) - \frac{1}{2}\sum_{k=1}^{5}\left[\tilde{\alpha}_k|\tilde{\lambda}_k|(1-\Phi(\tilde{\theta}_k)(1-|\tilde{\nu}_k|))\tilde{\mathbf{e}}_k\right]_{i+\frac{1}{2}}.$$

The inhomogeneous terms not containing first order derivatives, $\mathbf{S}$, are approximated using a pointwise approach,

$$\mathbf{S}_i^n = \begin{bmatrix} 0 \\ -\beta(u_g - u_s) \\ 0 \\ \frac{\beta}{\rho_s}(u_g - u_s) \\ -\frac{2}{\rho_s}\beta T_s \end{bmatrix}_i^n$$

and the inhomogeneous terms containing first order derivatives, $\mathbf{R}$, are approximated by using an upwind characteristic (CP) method,

$$\mathbf{R}_i^* = \mathbf{R}^-_{i+\frac{1}{2}} + \mathbf{R}^+_{i-\frac{1}{2}}, \tag{5.2}$$

where

$$\mathbf{R}^{\pm}_{i+\frac{1}{2}} = \frac{1}{2}\sum_{k=1}^{5}\left[\tilde{\beta}_k\tilde{\mathbf{e}}_k(1 \pm \operatorname{sgn}(\tilde{\lambda}_k)(1-\Phi(\tilde{\theta}_k)(1-|\tilde{\nu}_k|)))\right]_{i+\frac{1}{2}}.$$

The step sizes in space and time are Δx and Δt with i and n denoting the spatial and time grid number, respectively. The upstream and downstream boundaries are at x_0 and x_I (I is the total number of spatial grid points), t_N is the final time,

$$s = \frac{\Delta t}{\Delta x}, \quad \tilde{\nu}_k = s\tilde{\lambda}_k, \quad \tilde{\theta}_k = \frac{(\tilde{\alpha}_k)_{J+\frac{1}{2}}}{(\tilde{\alpha}_k)_{J+\frac{1}{2}}}, \quad J = i - \operatorname{sgn}(\tilde{\nu}_k)_{i+\frac{1}{2}},$$

and either the minmod flux-limiter [31],

$$\Phi(\theta) = \max(0, \min(1, \theta)), \tag{5.3}$$

or the van Leer [33] flux-limiter,

$$\Phi(\theta) = \frac{|\theta| + \theta}{1 + |\theta|}, \tag{5.4}$$

is used.

To ensure the scheme remains stable, the time step is calculated using

$$\Delta t = \frac{\nu \Delta x}{\max(|\lambda|)},$$

where $\max(|\lambda|)$ is the maximum wave speed and $\nu \leq 1$ is the required Courant number.

The scheme is an adapted form of Roe's scheme [26], which uses piecewise constant data to represent the domain and can be viewed as a family of Riemann problems due to a small discontinuity being present between each neighbouring cell $(\mathbf{w}_R, \mathbf{w}_L)$. This allows the system of homogeneous conservation laws,

$$\mathbf{w}_t + \mathbf{F}_x = 0$$

to be rewritten as a linearised Riemann problem,

$$\mathbf{w}_t + \tilde{\mathbf{A}}(\mathbf{w}_R, \mathbf{w}_L)\mathbf{w}_x = 0,$$

where the Jacobian $\tilde{\mathbf{A}}$ is constant locally. The numerical solution of the resulting linear problem requires an appropriate Roe averaged (denoted by $\tilde{\ }$) Jacobian matrix, determined by solving

$$\Delta \mathbf{F} = \sum_{k=1}^{5} \tilde{\alpha}_k \tilde{\lambda}_k \tilde{\mathbf{e}}_k = \tilde{\mathbf{A}} \Delta \mathbf{w},$$

whilst ensuring that the u-properties of Roe are satisfied. The Roe averaged eigenvalues $(\tilde{\lambda})$ and eigenvectors $(\tilde{\mathbf{e}})$ are then calculated from the Roe averaged Jacobian. The decomposition,

$$\Delta \mathbf{w} = \sum_{k=1}^{5} \tilde{\alpha}_k \tilde{\mathbf{e}}_k \quad \text{and} \quad \frac{1}{\Delta x} \sum_{k=1}^{5} \tilde{\beta}_k \tilde{\mathbf{e}}_k = \tilde{\mathbf{R}}$$

where $\Delta \mathbf{w} = \mathbf{w}_R - \mathbf{w}_L$, is then used to obtain the wave strengths $(\tilde{\alpha})$ and inhomogeneous values $(\tilde{\beta})$.

A full derivation of the Roe averages for all formulations is presented in Appendix A and a summary is given in Table 5.1, where the superscripts denote the corresponding formulation. The high resolution scheme can now be used to approximate the different systems of equations arising from the various formulations.

We are now in a position to obtain numerical solutions of the four systems of equations for a variety of test problems and to compare the results. This allows us to determine which formulation is the most robust and whether the two models produce different results.

6 Numerical Results

We now investigate the behaviour of the different models and the high resolution scheme for the gas-solid flow as discussed in Section 2.2. In order to compare the different models, we consider a variety of test cases all of which consist of a domain OP, 100 m long. Unless stated otherwise, the high resolution scheme is used with $\Delta x = 1$ m (i.e. 100 grid points) and a Courant number $\nu = 0.8$.

We only solve the models when they are hyperbolic and require appropriate initial and boundary conditions for each test case. Unless otherwise stated, the numerical scheme uses free flow boundary conditions,

$$\mathbf{w}_{-i}^{n+1} = \mathbf{w}_0^n \quad \text{and} \quad \mathbf{w}_{I+i}^{n+1} = \mathbf{w}_I^n,$$

For the regime under investigation, the gas phase is subcritical whilst the solids phase can either be subcritical or supercritical. Thus, if physical boundary conditions are required only three (if the solids phase is subcritical) or four (if the solids phase is supercritical) can be prescribed at the upstream boundary.

6.1 Advection Test Problem

The first test case is a simple solids advection problem where an analytical solution can be obtained, which is very useful in determining that the numerical scheme is behaving appropriately. The analytical solution is derived by assuming that the gas density and both phase velocities are constants,

$$\rho_g(x,t) = R \quad \text{and} \quad u_g(x,t) = u_s(x,t) = U,$$

then both models simplify to

$$(\epsilon_s)_t + U(\epsilon_s)_x = 0, \quad p_s(x,t) = P \quad \text{and} \quad (T_s)_t + U(T_s)_x = 0,$$

Formulation	Scheme	$\Delta x = 1$	0.5	0.1	0.05	0.01
AS	FO	0.9775960	0.7685596	0.3233380	0.1925014	0.0460192
AP	FO	0.9775960	0.7685596	0.3233380	0.1925014	0.0460192
BS	FO	0.9775960	0.7685596	0.3233380	0.1925014	0.0460192
BP	FO	0.9775960	0.7685596	0.3233380	0.1925014	0.0460192
AS	HR	0.5624180	0.2785775	0.0277546	0.0079563	0.0003928
AP	HR	0.5624181	0.2785775	0.0277546	0.0079563	0.0003928
BS	HR	0.5624180	0.2785775	0.0277546	0.0079563	0.0003928
BP	HR	0.5624180	0.2785775	0.0277546	0.0079563	0.0003928

Table 6.1: The L_1 error of the scheme at $t = 10$ s.

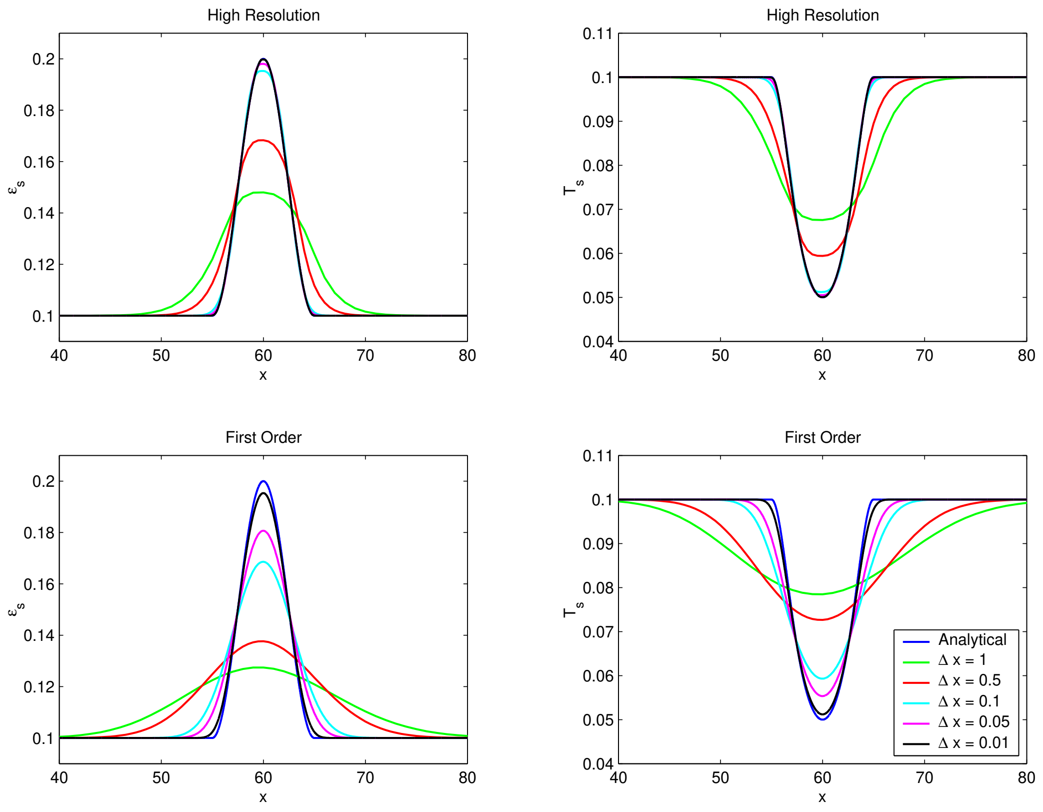

Figure 6.1: Results of the Advection Test Problem at $t = 10$ s (Formulation AS).

where P is a constant. Thus, we obtain the analytical solution

$$\epsilon_s(x,t) = \epsilon_s(x - Ut, 0) \quad \text{and} \quad T_s(x,t) = \frac{P}{\epsilon_s}.$$

To simulate a solids pulse propagating downstream, we use the initial conditions,

$$\epsilon_s(x,0) = \begin{cases} 0.1 + 0.1\sin^2\left(\frac{\pi}{10}(x-5)\right) & \text{if } 5 \le x \le 15 \\ 0.1 & \text{otherwise} \end{cases}$$

with

$$R = 1.2885, \quad U = 5 \quad \text{and} \quad P = 0.01.$$

Table 6.1 denotes the L_1 error,

$$||\mathbf{E}||_1 = \Delta x \sum_{i=0}^{I} |\mathbf{E}_i^N|, \quad \text{where} \quad \mathbf{E} = \mathbf{w}(x,t) - \mathbf{w}_i^n$$

for the sum of all variables at $t = 10$ s (N is the total number of time steps required to reach this time) for both first order ($\Phi = 0$) and high resolution (with minmod limiter) versions of the scheme (5.1). The numerical solution converges to the analytical solution as the mesh size is reduced. Notice that the results of all formulations are almost identical with the first order results producing a higher L_1 error than the high resolution scheme. These findings are verified in Figure 6.1, where it is clear that the first order scheme suffers more from diffusion. Thus, the results show that the high resolution scheme is superior to the first order version of the scheme.

6.2 Square Pulse Test Problem

For the second test case, we simulate a square pulse of solids in the centre of the domain, which is at rest. In this simple simulation, we imagine that "walls" at $x = 40$ m and $x = 60$ m confine the solids to the region $40 < x < 60$ of the domain and they are kept in suspension by a "stirrer". The "walls" are then removed at time $t = 0$ and the solids are allowed to move freely. The initial conditions for this test case consists of

$$\rho_g(x,0) = 1.2885, \quad u_g(x,0) = u_s(x,0) = 0, \quad T_s(x,0) = 0.1\epsilon_s(x,0)$$

and

$$\epsilon_s(x,0) = \begin{cases} 0.2 & \text{if } 40 \le x \le 60, \\ 0.1 & \text{otherwise.} \end{cases}$$

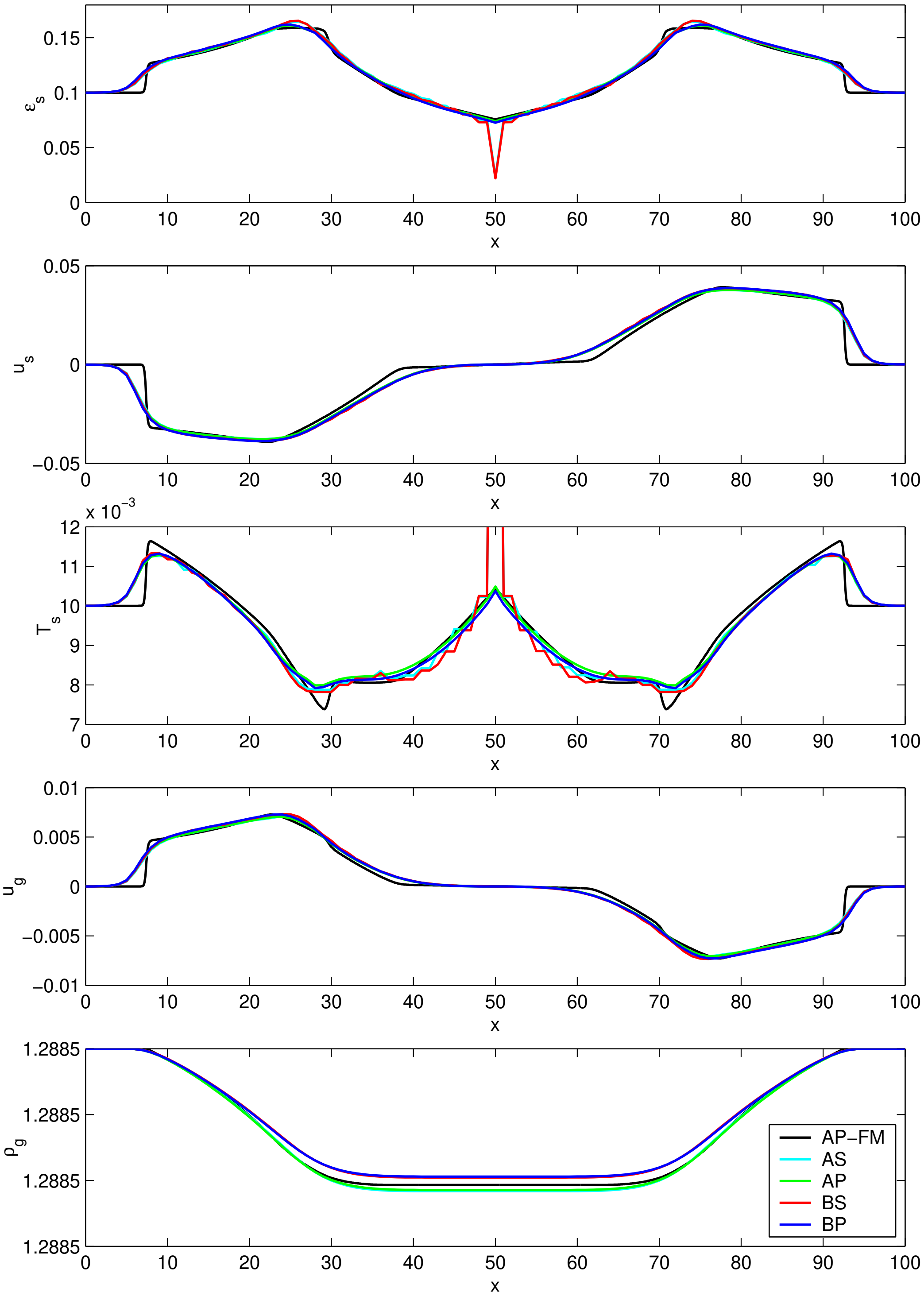

Figure 6.2: Results for the Square Pulse Test Problem at $t = 200$ s.

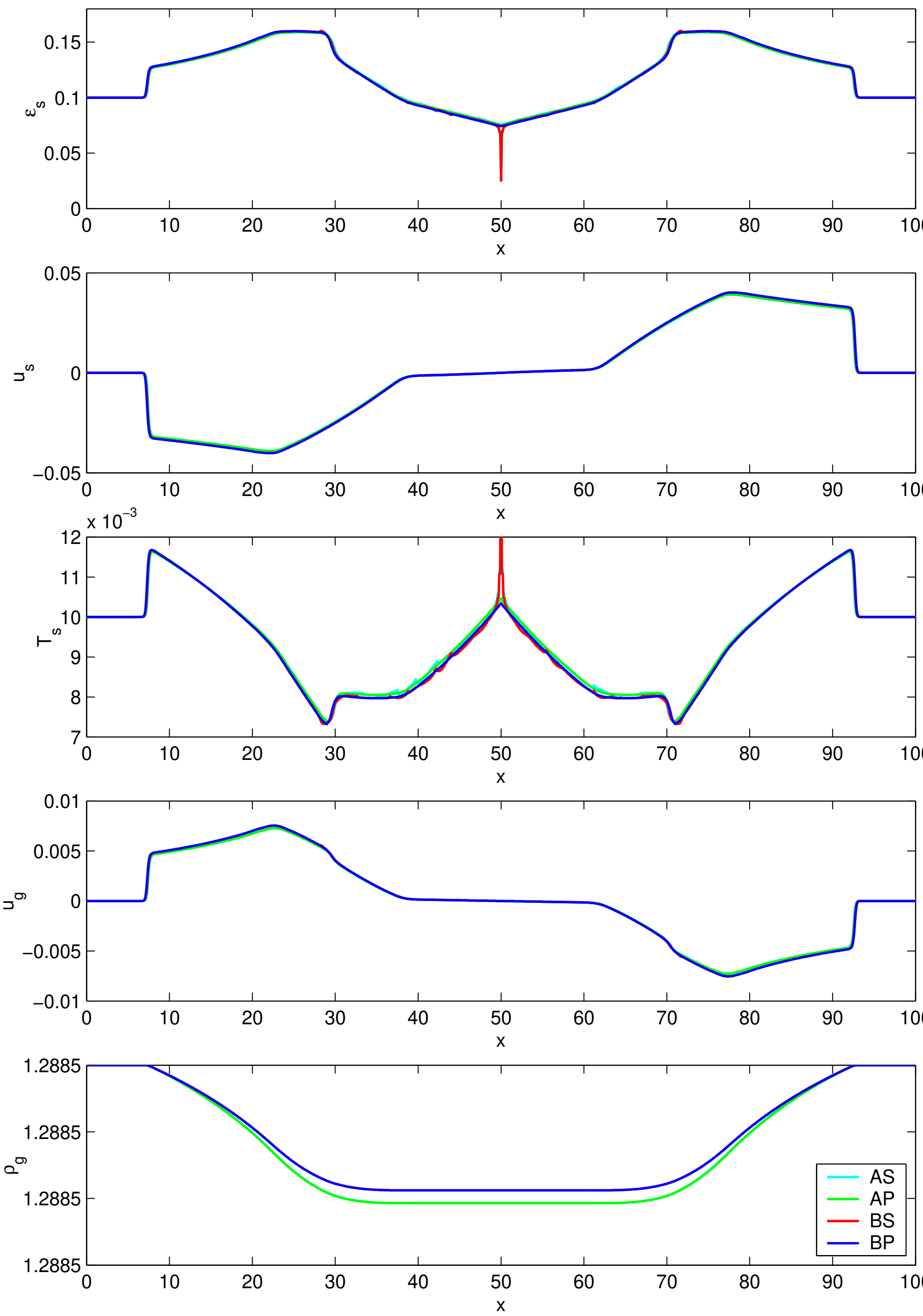

Figure 6.3: Results for the Square Pulse Test Problem at $t = 200$ s (Fine Mesh).

Figures 6.2 & 6.3 illustrate the results for the different formulations using the Square Pulse Test Problem at $t = 200$ s. The fine mesh results were obtained using a step size of $\Delta x = 0.1$. All formulations produced practically identical results. However, it is to be noted that there is a numerical problem with the systems AS and BS. This seems to be caused by the term $-p_s(u_s)_x$ and is due to the stagnation point (at $x = 50$ m). A similar problem arises in single-phase gas dynamics in cases where the entropy condition is violated, see LeVeque [21] for more information. Moreover, it also occurs with the first order version of the scheme, $\Phi = 0$, thus applying limiters for the approximation of the inhomogeneous terms with first order derivatives is not the cause of the problem. In our case, however, it is the approximation of the inhomogeneous term in the granular temperature equation which appears to be responsible. It is rectified by using the systems AP and BP. Figure 6.4 illustrates the evolution of the test case for the fine mesh results using Formulation AP. Initially the square pulse starts to collapse with two waves propagating in opposite directions. The shapes of the waves are such that after 40 seconds a peak has appeared at each side of the square pulse in the granular temperature. Although it appears to be similar to an entropy violation, the HLLE scheme [6] was used as a check and produced identical results to those displayed here, indicating that there is no entropy violation. Also notice that at 200 seconds, the solids pressure is constant in the region $x = 40$ to 60 m and the solution seems to be settling down to a steady state.

6.3 Steady State Test Problem

The simplest family of steady state solutions are obtained by setting the velocities equal, i.e. $u_g = u_s$. The inter-phase drag force is then zero. For our purposes, a better steady state solution of the model is one with different velocities so that the drag force is included.

For the general system, a steady state solution exists if the discharges for both phases are constant, i.e.

$$Q_g = \epsilon_g \rho_g u_g \quad \text{and} \quad Q_s = \epsilon_s \rho_s u_s,$$

and the three ordinary differential equations

$$Q_g(u_g)_x + \omega_1(p_g)_x + \omega_2(p_s)_x = -\beta(u_g - u_s), \tag{6.1a}$$

$$Q_s(u_s)_x + \omega_3(p_g)_x + \omega_4(p_s)_x = \beta(u_g - u_s) \tag{6.1b}$$

and

$$Q_s(T_s)_x = -\frac{2}{3}\left(p_s(u_s)_x + 3\beta T_s\right). \tag{6.1c}$$

are satisfied.

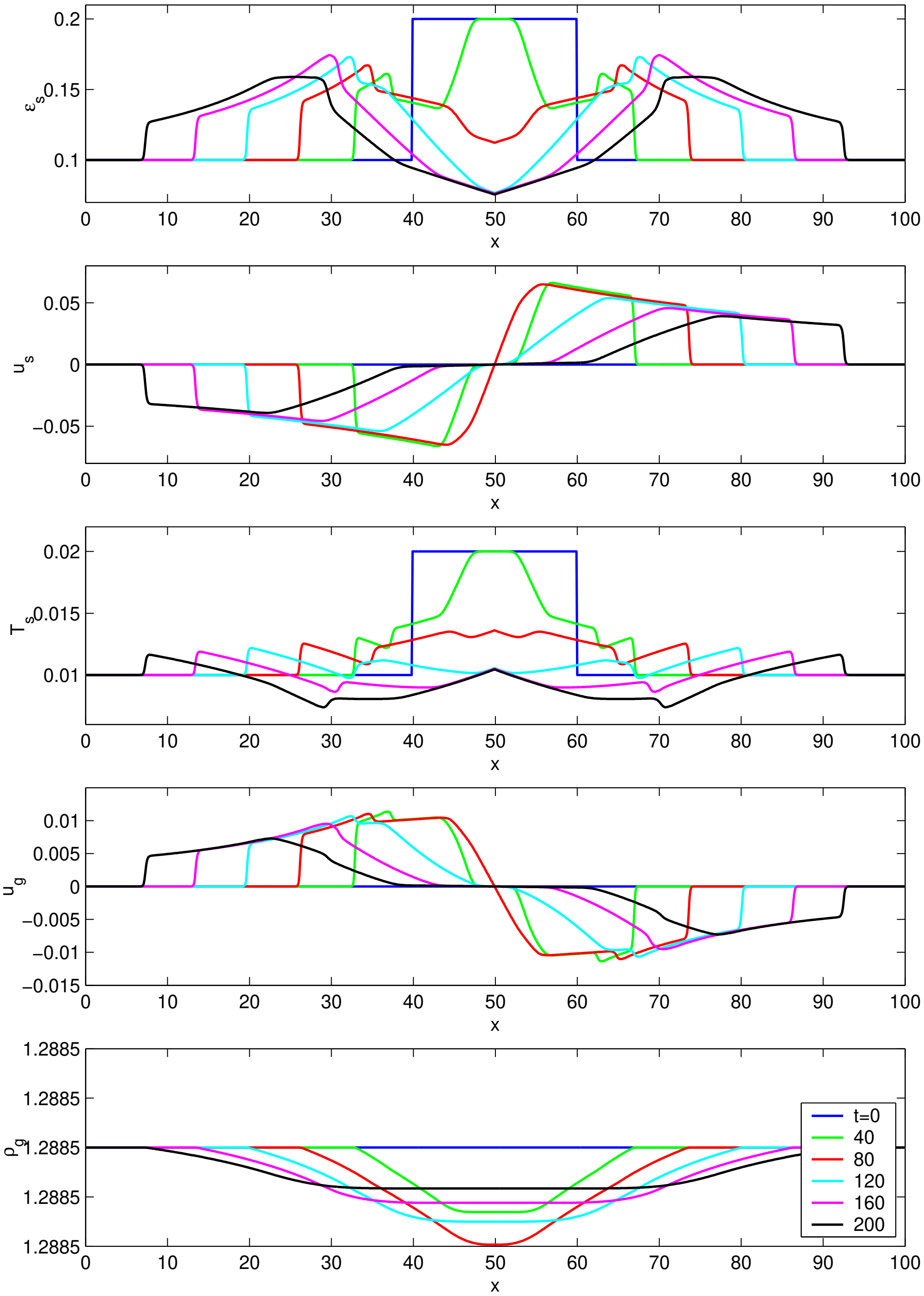

Figure 6.4: Fine Mesh Results of Formulation AP at $t = 0$ to 200 s.

To obtain a steady state solution for non-equal velocities, different velocities are imposed at the upstream boundary and the scheme iterated until a steady state has been reached. The initial conditions are

$$\rho_g(x,0) = 1.2885, \quad u_g(x,0) = u_g^0,$$

$$\epsilon_s(x,0) = 0.1, \quad u_s(x,0) = 1 \quad \text{and} \quad T_s(x,0) = 0.1,$$

with boundary conditions

$$\rho_g(100,t) = 1.2885, \quad u_g(0,t) = u_g^0, \tag{6.2a}$$

$$\epsilon_s(0,t) = 0.1, \quad u_s(0,t) = 1 \quad \text{and} \quad T_s(0,t) = 0.001. \tag{6.2b}$$

The condition for a steady state to have been reached is

$$|\mathbf{w}_i^{n+1} - \mathbf{w}_i^n| \leq \text{tol} \quad \forall i, \tag{6.3}$$

where tol = 1E-8. However, if the scheme has not converged within $t = 150$ s (by which time the solution is very close to the steady state solution), convergence is stopped and the number of unconverged points is given.

Figures 6.5 & 6.6 illustrate a comparison of the different models using either $u_g^0 = 1.5$ m/s or $u_g^0 = 5$ m/s, respectively. All models were approximated using the high resolution scheme either the minmod limiter for $u_g^0 = 1.5$ or the van Leer limiter for $u_g^0 = 5$. Two spatial step sizes were used: the standard $\Delta x = 1$ m and a Fine Mesh (FM) of $\Delta x = 0.1$ m.

The results show that as the gas velocity is increased, the gradient of the variables at the upstream boundary increases due to the drag force dominating the pressure gradient terms as the difference between the velocities becomes larger. From equations (6.1a) and (6.1b)

$$(u_g - u_s)_x + \left(\frac{\omega_1}{Q_g} - \frac{\omega_3}{Q_s}\right)(p_g)_x + \left(\frac{\omega_2}{Q_g} - \frac{\omega_4}{Q_s}\right)(p_s)_x = -\beta^0\left(\frac{Q_g + Q_s}{Q_g Q_s}\right)(u_g - u_s)^2,$$

where the drag force has been simplified and β^0 is assumed to be a constant

$$\beta^0 = \frac{3C_D}{4d_s}\rho_g^0\epsilon_g^0\epsilon_s^0,$$

obtained from the boundary values (denoted by a ^{0} superscript). Supposing the drag force is large compared with the pressure gradient terms, the latter may be neglected and we obtain an equation for the difference in velocities

$$(u_g - u_s)_x = -\beta^0\left(\frac{Q_g + Q_s}{Q_g Q_s}\right)(u_g - u_s)^2$$

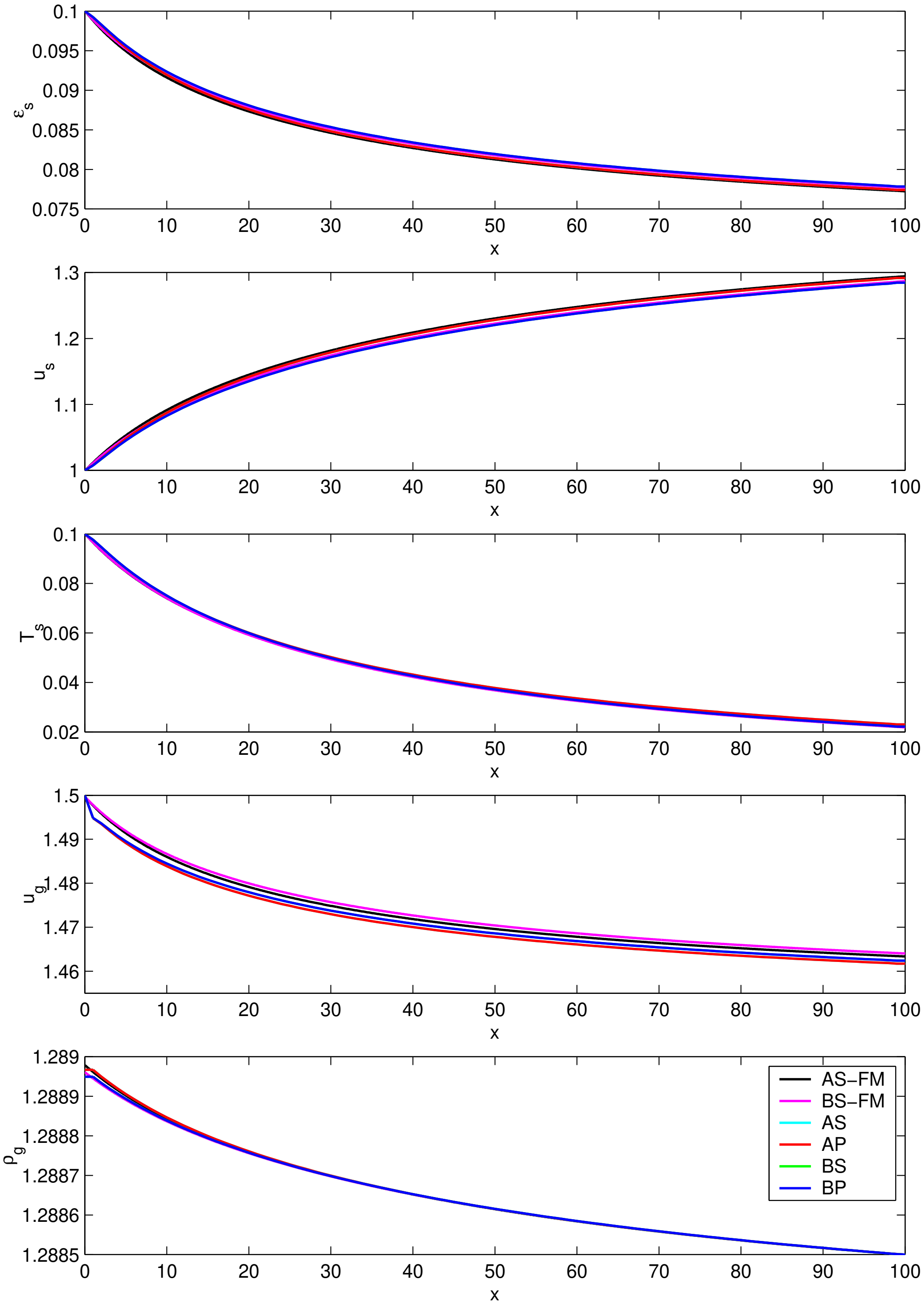

Figure 6.5: Results for the Steady State Test Problem s with $u_g^0 = 1.5$ m/s.

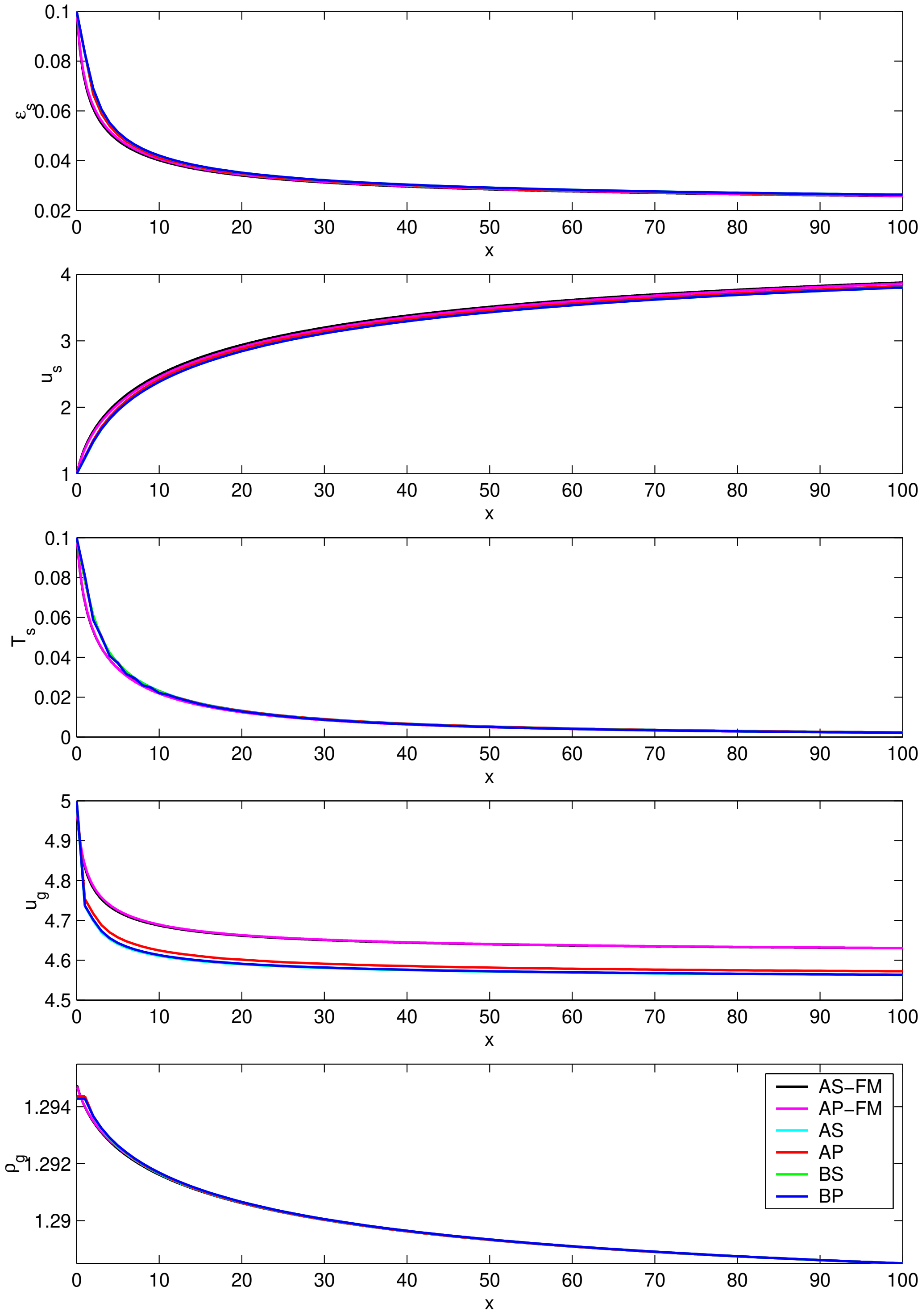

Figure 6.6: Results for the Steady State Test Problem with $u_g^0 = 5$ m/s.

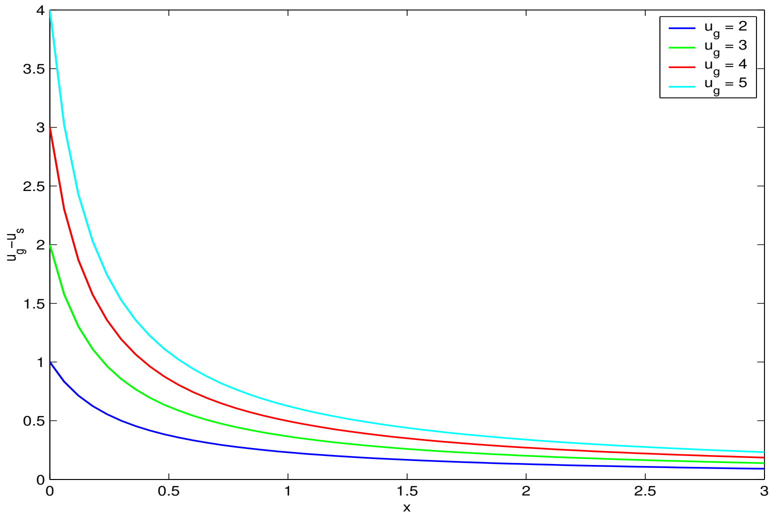

Figure 6.7: Illustration of the significance of the drag force.

with solution

$$u_g - u_s = \frac{u_g^0 - u_s^0}{\beta^0 \left(\frac{Q_g+Q_s}{Q_g Q_s}\right)(u_g^0 - u_s^0)x + 1}.$$

Figure 6.7 illustrates this equation for the boundary values (6.2) with $u_g^0 = 2$ to 5. Notice that there is a vertical asymptote close to the origin,

$$x^* = \frac{-1}{\beta^0 \left(\frac{Q_g+Q_s}{Q_g Q_s}\right)(u_g^0 - u_s^0)},$$

which gets closer to the origin as the difference between $u_g - u_s$ increases.

As the difference between the velocities increases at the upstream boundary, a kink becomes discernible (in the gas variables) a distance Δx, (one grid point) away from the upstream boundary and is due to the effect of the drag force on the gradient in the variables at the upstream boundary. As the difference between the two velocities increases, the gradient increases at the upstream boundary and the kink becomes more prominent. This may be rectified by using a finer space mesh so that the gradient is more accurately calculated. As the difference between the velocities increases, e.g. $u_g - u_s > 5$, the drag force term becomes “stiff” and the scheme becomes unstable.

This test case is sensitive to the type of flux-limiter. If the min mod limiter (5.3) is used then the scheme requires a larger value of tol as $u_g^0 \to 5$ in order for (6.3) to be satisfied.

If the van Leer limiter is used (5.4), the scheme (with formulations S) quickly satisfies (6.3) with the given value of tol = 1E-8. Unfortunately, the P formulations were unable to converge within $t = 150$ s when $u_g^0 = 5$, but the results still look acceptable. This seems to indicate that the scheme is more stable with the van Leer limiter than the minmod limiter and the lack of convergence of the P formulations is probably due to the "stiff" drag force term.

Concerning the inter-phase drag force, in Model B, if gravity is present Gidaspow [8] deduced that the drag force coefficient must be replaced with

$$\beta_B = \beta_A \epsilon_s^{-1}$$

in order for Archimedes principle to be satisfied. In the problems considered here, gravity is absent and so the same drag force coefficient was used in both models. Boemer *et al.* [2] also illustrated a difference between the models for certain test cases of 2D fluidized beds. They deduced that Model B results in a physical modification of the problem which can lead to an artificial increase in the forces carrying the particles. Moreover, even though Model A is deemed to be more physically correct than Model B, Boemer *et al.* also demonstrated that Model B produced numerical results that were closer to experiments than Model A.

7 Conclusion

In this paper, we have investigated two standard Eulerian two-phase solid-gas flow models and applied a high resolution scheme to obtain numerical approximations for a variety of test cases. The results for all formulations were promising with the exception of a numerical problem occurring in the results of the S formulations. However the problem can be solved by using the product rule to re-write the term $-p_s(u_s)_x$ thus, obtaining the P formulations.

We have demonstrated that Model A is hyperbolic for a region of small relative velocities, which is due the inclusion of the solids pressure in the solids phase momentum equation. The size of the region is dependent on the values of ϵ_s, T_s and ρ_g. Model B is unconditionally hyperbolic. For small relative velocities, the regime of physical interest, Model A remains well-posed, although it becomes ill-posed as $T_s \to 0$.

For the test cases investigated here, the gas density ρ_g remains almost constant and the gradient of gas pressure is small. Models A and B only differ due to the gas pressure derivatives thus, there is little difference between them if the gradient of the gas pressure term is negligible.

A final conclusion is that both Models A and B can be accurately approximated using the high resolution scheme presented in this paper.

Acknowledgements

The first author would like to thank the **E**ngineering and **P**hysical **S**cience **R**esearch **C**ouncil for their funding.

A Derivation of Roe Average Values

The numerical scheme discussed in Section 5 is based on Roe's scheme [26] and thus, requires Roe averaged values. In this section, we briefly outline the derivation of the Roe averaged values for the general system.

We require a Roe averaged Jacobian matrix, $\tilde{\mathbf{A}}(\mathbf{w}_L, \mathbf{w}_R)$, which satisfies the following u-properties [26],

- $\tilde{\mathbf{A}}(\mathbf{w}_L, \mathbf{w}_R)$ must be diagonalisable with real eigenvalues (hyperbolicity);
- $\tilde{\mathbf{A}}(\mathbf{w}_L, \mathbf{w}_R) \rightarrow \tilde{\mathbf{A}}(\mathbf{w})$ as $\mathbf{w}_L$,$\mathbf{w}_R \rightarrow \mathbf{w}$ (consistency);
- $\Delta\mathbf{F} = \tilde{\mathbf{A}}(\mathbf{w}_L, \mathbf{w}_R)\Delta\mathbf{w}$ (conservation).

We obtain such a Roe averaged Jacobian by using the conservation u-property to obtain Roe averaged values of the variables, which can then be used to obtain the eigenvalues and eigenvectors.

A.1 Roe Averages

All Models must satisfy,

$$\Delta\mathbf{F} = \tilde{\mathbf{A}}\Delta\mathbf{w},$$

where for:

1. Models AS and BS,

$$\tilde{\mathbf{A}} = \begin{bmatrix} 0 & 1 & 0 & 0 & 0 \\ \tilde{\epsilon}_g^{-1}\tilde{c}_g^2 - \tilde{u}_g^2 & 2\tilde{u}_g & \tilde{\rho}_g\tilde{\epsilon}_g^{-1}\tilde{c}_g^2 & 0 & 0 \\ 0 & 0 & 0 & 1 & 0 \\ 0 & 0 & -\tilde{u}_s^2 & 2\tilde{u}_s & 1 \\ 0 & 0 & -\tilde{u}_s\tilde{T}_s & \tilde{T}_s & \tilde{u}_s \end{bmatrix} \quad \text{and} \quad \mathbf{F} = \begin{bmatrix} \epsilon_g\rho_g u_g \\ \epsilon_g\rho_g u_g^2 + p_g \\ \epsilon_s u_s \\ \epsilon_s u_s^2 + \epsilon_s T_s \\ \epsilon_s u_s T_s \end{bmatrix}.$$

2. Models AP and BP,

$$\tilde{\mathbf{A}} = \begin{bmatrix} 0 & 1 & 0 & 0 & 0 \\ \tilde{\epsilon}_g^{-1}\tilde{c}_g^2 - \tilde{u}_g^2 & 2\tilde{u}_g & \tilde{\rho}_g\tilde{\epsilon}_g^{-1}\tilde{c}_g^2 & 0 & 0 \\ 0 & 0 & 0 & 1 & 0 \\ 0 & 0 & -\tilde{u}_s^2 & 2\tilde{u}_s & 1 \\ 0 & 0 & -\frac{5}{3}\tilde{u}_s\tilde{T}_s & \frac{5}{3}\tilde{T}_s & \frac{5}{3}\tilde{u}_s \end{bmatrix} \quad \text{and} \quad \mathbf{F} = \begin{bmatrix} \epsilon_g\rho_g u_g \\ \epsilon_g\rho_g u_g^2 + p_g \\ \epsilon_s u_s \\ \epsilon_s u_s^2 + \epsilon_s T_s \\ \frac{5}{3}\epsilon_s u_s T_s \end{bmatrix}.$$

All of these Models result in ensuring that the following equations are satisfied:

$$\Delta(\epsilon_g\rho_g u_g) = \Delta(\epsilon_g\rho_g u_g), \tag{A.1a}$$

$$\Delta(\epsilon_g\rho_g u_g^2) + \Delta p_g = (\tilde{c}_g^2\tilde{\epsilon}_g^{-1} - \tilde{u}_g^2)\Delta(\epsilon_g\rho_g) + 2\tilde{u}_g\Delta(\epsilon_g\rho_g u_g) + \tilde{\rho}_g\tilde{\epsilon}_g^{-1}\tilde{c}_g^2\Delta\epsilon_s, \tag{A.1b}$$

$$\Delta(\epsilon_s u_s) = \Delta(\epsilon_s u_s), \tag{A.1c}$$

$$\Delta(\epsilon_s u_s^2) + \Delta(\epsilon_s T_s) = -\tilde{u}_s^2\Delta\epsilon_s + 2\tilde{u}_s\Delta(\epsilon_s u_s) + \Delta(\epsilon_s T_s) \tag{A.1d}$$

and

$$\Delta(\epsilon_s u_s T_s) = -\tilde{u}_s\tilde{T}_s\Delta\epsilon_s + \tilde{T}_s\Delta(\epsilon_s u_s) + \tilde{u}_s\Delta(\epsilon_s T_s). \tag{A.1e}$$

Clearly, equations (A.1a) and (A.1c) are automatically satisfied. To obtain Roe average values of the velocities, we let

$$\tilde{u}_g^2\Delta(\epsilon_g\rho_g) - 2\tilde{u}_g\Delta(\epsilon_g\rho_g u_g) + \Delta(\epsilon_g\rho_g u_g^2) = 0$$

and

$$\tilde{u}_s^2\Delta\epsilon_s - 2\tilde{u}_s\Delta(\epsilon_s u_s) + \Delta(\epsilon_s u_s^2) = 0.$$

Thus, by obtaining the roots of these two quadratic equations (of $\tilde{u}_k$) we can use one of the roots for the Roe averaged value,

$$\tilde{u}_g = \frac{\sqrt{(\epsilon_g\rho_g)_L}(u_g)_L + \sqrt{(\epsilon_g\rho_g)_R}(u_g)_R}{\sqrt{(\epsilon_g\rho_g)_L} + \sqrt{(\epsilon_g\rho_g)_R}} \quad \text{and} \quad \tilde{u}_s = \frac{\sqrt{(\epsilon_s)_L}(u_s)_L + \sqrt{(\epsilon_s)_R}(u_s)_R}{\sqrt{(\epsilon_s)_L} + \sqrt{(\epsilon_s)_R}}.$$

We can now obtain,

$$\tilde{T}_s = \frac{\sqrt{(\epsilon_s)_L}(T_s)_L + \sqrt{(\epsilon_s)_R}(T_s)_R}{\sqrt{(\epsilon_s)_L} + \sqrt{(\epsilon_s)_R}}$$

by substituting $\tilde{u}_s$ into (A.1e) and simplifying.

Thus, we only have

$$\tilde{\epsilon}_g\Delta p_g = \tilde{c}_g^2(\Delta(\epsilon_g\rho_g) - \tilde{\rho}_g\Delta\epsilon_g),$$

which can be simplified by letting

$$\tilde{c}_g^2 = \frac{\Delta p_g}{\Delta\rho_g}$$

thus,

$$\Delta(\epsilon_g\rho_g) = \tilde{\epsilon}_g\Delta\rho_g + \tilde{\rho}_g\Delta\epsilon_g.$$

Here, we have two options:

$$\tilde{\epsilon}_k = \frac{1}{2}((\epsilon_k)_L + (\epsilon_k)_R) \quad \text{and} \quad \tilde{\rho}_g = \frac{1}{2}((\rho_g)_L + (\rho_g)_R) \tag{A.2}$$

or

$$\tilde{\epsilon}_k = \sqrt{(\epsilon_k)_L(\epsilon_k)_R} \quad \text{and} \quad \tilde{\rho}_g = \frac{\sqrt{(\epsilon_g)_L}(\rho_g)_L + \sqrt{(\epsilon_g)_R}(\rho_g)_R}{\sqrt{(\epsilon_g)_L} + \sqrt{(\epsilon_g)_R}}. \tag{A.3}$$

Thus, all the Roe average values have been obtained. Notice that these values ensure that the other u-properties are satisfied.

A.2 Eigenvalues & Eigenvectors

The eigenvalues and eigenvectors are obtained directly from the corresponding Roe averaged Jacobian matrix. We can easily obtain the eigenvalues for:

1. Models AS and BS,

$$\tilde{\lambda}_{1,2} = \tilde{u}_g \mp \tilde{c}_g\sqrt{\tilde{\epsilon}_g^{-1}}, \quad \tilde{\lambda}_3 = \tilde{u}_s \quad \text{and} \quad \tilde{\lambda}_{4,5} = \tilde{u}_s \mp \sqrt{\tilde{T}_s}.$$

2. Models AP and BP,

$$\tilde{\lambda}_{1,2} = \tilde{u}_g \mp \tilde{c}_g \sqrt{\tilde{\epsilon}_g^{-1}}, \quad \tilde{\lambda}_3 = \tilde{u}_s \quad \text{and} \quad \tilde{\lambda}_{4,5} = \frac{4}{3}\tilde{u}_s \mp \frac{1}{3}\sqrt{15\tilde{T}_s + \tilde{u}_s^2}.$$

For simplicity (and computational efficiency), the eigenvectors are determined in terms of the numerical eigenvalues and are obtained by solving:

1. Models AS and BS,

$$\begin{bmatrix} -\tilde{\lambda} & 1 & 0 & 0 & 0 \\ \tilde{\epsilon}_g^{-1}\tilde{c}_g^2 - \tilde{u}_g^2 & 2\tilde{u}_g - \tilde{\lambda} & \tilde{\rho}_g\tilde{\epsilon}_g^{-1}\tilde{c}_g^2 & 0 & 0 \\ 0 & 0 & -\tilde{\lambda} & 1 & 0 \\ 0 & 0 & -\tilde{u}_s^2 & 2\tilde{u}_s - \tilde{\lambda} & 1 \\ 0 & 0 & -\tilde{u}_s\tilde{T}_s & \tilde{T}_s & \tilde{u}_s - \tilde{\lambda} \end{bmatrix} \begin{bmatrix} 1 \\ e_2 \\ e_3 \\ e_4 \\ e_5 \end{bmatrix} = 0.$$

2. Models AP and BP,

$$\begin{bmatrix} -\tilde{\lambda} & 1 & 0 & 0 & 0 \\ \tilde{\epsilon}_g^{-1}\tilde{c}_g^2 - \tilde{u}_g^2 & 2\tilde{u}_g - \tilde{\lambda} & \tilde{\rho}_g\tilde{\epsilon}_g^{-1}\tilde{c}_g^2 & 0 & 0 \\ 0 & 0 & -\tilde{\lambda} & 1 & 0 \\ 0 & 0 & -\tilde{u}_s^2 & 2\tilde{u}_s - \tilde{\lambda} & 1 \\ 0 & 0 & -\frac{5}{3}\tilde{u}_s\tilde{T}_s & \frac{5}{3}\tilde{T}_s & \frac{5}{3}\tilde{u}_s - \tilde{\lambda} \end{bmatrix} \begin{bmatrix} 1 \\ e_2 \\ e_3 \\ e_4 \\ e_5 \end{bmatrix} = 0.$$

Thus,

$$e_2 = \tilde{\lambda}, \tag{A.4a}$$

$$\tilde{\epsilon}_g^{-1}\tilde{c}_g^2 - \tilde{u}_g^2 + (2\tilde{u}_g - \tilde{\lambda})e_2 + \tilde{\rho}_g\tilde{\epsilon}_g^{-1}\tilde{c}_g^2 e_3 = 0, \tag{A.4b}$$

$$e_4 = \tilde{\lambda}e_3, \tag{A.4c}$$

$$-\tilde{u}_s^2 e_3 + (2\tilde{u}_s - \tilde{\lambda})e_4 + e_5 = 0 \tag{A.4d}$$

and either

$$-\tilde{u}_s\tilde{T}_s e_3 + \tilde{T}_s e_4 + (\tilde{u}_s - \tilde{\lambda})e_5 = 0 \tag{A.4e}$$

for Models AS and BS or

$$-\frac{5}{3}\tilde{u}_s\tilde{T}_s e_3 + \frac{5}{3}\tilde{T}_s e_4 + (\frac{5}{3}\tilde{u}_s - \tilde{\lambda})e_5 = 0 \tag{A.4f}$$

for Models AP and BP. Now, by substituting (A.4a) into (A.4b), we obtain

$$e_3 = \frac{\tilde{u}_g^2\tilde{\epsilon}_g - \tilde{c}_g^2 - (2\tilde{u}_g - \tilde{\lambda})\tilde{\epsilon}_g\tilde{\lambda}}{\tilde{\rho}_g\tilde{c}_g^2} = \frac{(\tilde{\lambda} - \tilde{u}_g)^2\tilde{\epsilon}_g - \tilde{c}_g^2}{\tilde{\rho}_g\tilde{c}_g^2}.$$

Also, by substituting (A.4c) into (A.4d), we obtain

$$e_5 = e_3(\tilde{\lambda} - \tilde{u}_s)^2.$$

Hence, we obtain

$$\tilde{\mathbf{e}}_{1,2} = \begin{bmatrix} 1 \\ \tilde{\lambda}_{1,2} \\ 0 \\ 0 \\ 0 \end{bmatrix} \quad \text{and} \quad \tilde{\mathbf{e}}_{3,4,5} = \begin{bmatrix} 1 \\ \tilde{\lambda}_{3,4,5} \\ \tilde{d}_{3,4,5} \\ \tilde{\lambda}_{3,4,5}\tilde{d}_{3,4,5} \\ \tilde{d}_{3,4,5}(\tilde{\lambda}_{3,4,5} - \tilde{u}_s)^2 \end{bmatrix},$$

where

$$\tilde{d}_k = \frac{(\tilde{\lambda}_k - \tilde{u}_g)^2\tilde{\epsilon}_g - \tilde{c}_g^2}{\tilde{\rho}_g\tilde{c}_g^2}.$$

A.3 Wave Strengths

We obtain wave strengths through the decomposition,

$$\Delta\mathbf{w} = \sum_{k=1}^{5} \tilde{\alpha}_k\tilde{\mathbf{e}}_k,$$

which for all models results in solving

$$\Delta(\epsilon_g\rho_g) = \tilde{\alpha}_1 + \tilde{\alpha}_2 + \tilde{\alpha}_3 + \tilde{\alpha}_4 + \tilde{\alpha}_5, \tag{A.5a}$$

$$\Delta(\epsilon_g\rho_g u_g) = \tilde{\lambda}_1\tilde{\alpha}_1 + \tilde{\lambda}_2\tilde{\alpha}_2 + \tilde{\lambda}_3\tilde{\alpha}_3 + \tilde{\lambda}_4\tilde{\alpha}_4 + \tilde{\lambda}_5\tilde{\alpha}_5, \tag{A.5b}$$

$$\Delta\epsilon_s = \tilde{d}_3\tilde{\alpha}_3 + \tilde{d}_4\tilde{\alpha}_4 + \tilde{d}_5\tilde{\alpha}_5, \tag{A.5c}$$

$$\Delta(\epsilon_s u_s) = \tilde{\lambda}_3\tilde{d}_3\tilde{\alpha}_3 + \tilde{\lambda}_4\tilde{d}_4\tilde{\alpha}_4 + \tilde{\lambda}_5\tilde{d}_5\tilde{\alpha}_5 \tag{A.5d}$$

and

$$\Delta(\epsilon_s T_s) = \tilde{d}_3(\tilde{\lambda}_3 - \tilde{u}_s)^2\tilde{\alpha}_3 + \tilde{d}_4(\tilde{\lambda}_4 - \tilde{u}_s)^2\tilde{\alpha}_4 + \tilde{d}_5(\tilde{\lambda}_5 - \tilde{u}_s)^2\tilde{\alpha}_5 \tag{A.5e}$$

for $\tilde{\alpha}_k$. The algebraic expressions obtained by solving this set of simultaneous equations $\tilde{\alpha}_{1,2}$ are complicated. To keep the algebraic expressions in a compact form, we solve (A.5c), (A.5d) and (A.5e) to obtain $\tilde{\alpha}_{3,4,5}$,

$$\tilde{\alpha}_k = \frac{(\tilde{\lambda}_a\tilde{\lambda}_b - \tilde{u}_s^2)\Delta\epsilon_s - (\tilde{\lambda}_a + \tilde{\lambda}_b - 2\tilde{u}_s)\Delta(\epsilon_s u_s) + \Delta(\epsilon_s T_s)}{\tilde{d}_k(\tilde{\lambda}_k - \tilde{\lambda}_a)(\tilde{\lambda}_k - \tilde{\lambda}_b)}$$

where $k \neq a \neq b$, and then solve $\tilde{\alpha}_{1,2}$ in terms of the other wave strengths,

$$\tilde{\alpha}_{1,2} = \mp\frac{\tilde{\lambda}_3\tilde{\alpha}_3 + \tilde{\lambda}_4\tilde{\alpha}_4 + \tilde{\lambda}_5\tilde{\alpha}_5 - (\tilde{\alpha}_3 + \tilde{\alpha}_4 + \tilde{\alpha}_5 - \Delta(\epsilon_g\rho_g))\tilde{\lambda}_{2,1} - \Delta(\epsilon_g\rho_g u_g)}{\tilde{\lambda}_1 - \tilde{\lambda}_2}.$$

A.4 Inhomogeneous Terms

The values of $\tilde{\beta}_k$ are also determined from the decomposition,

$$\Delta x \tilde{\mathbf{R}} = \sum_{k=1}^{5} \tilde{\beta}_k \tilde{\mathbf{e}}_k,$$

which for the system results in solving

$$0 = \tilde{\beta}_1 + \tilde{\beta}_2 + \tilde{\beta}_3 + \tilde{\beta}_4 + \tilde{\beta}_5, \tag{A.6a}$$

$$\tilde{r}_2 = \tilde{\lambda}_1\tilde{\beta}_1 + \tilde{\lambda}_2\tilde{\beta}_2 + \tilde{\lambda}_3\tilde{\beta}_3 + \tilde{\lambda}_4\tilde{\beta}_4 + \tilde{\lambda}_5\tilde{\beta}_5, \tag{A.6b}$$

$$0 = \tilde{d}_3\tilde{\beta}_3 + \tilde{d}_4\tilde{\beta}_4 + \tilde{d}_5\tilde{\beta}_5, \tag{A.6c}$$

$$\tilde{r}_4 = \tilde{\lambda}_3\tilde{d}_3\tilde{\beta}_3 + \tilde{\lambda}_4\tilde{d}_4\tilde{\beta}_4 + \tilde{\lambda}_5\tilde{d}_5\tilde{\beta}_5 \tag{A.6d}$$

and

$$\tilde{r}_5 = \tilde{d}_3(\tilde{\lambda}_3 - \tilde{u}_s)^2\tilde{\beta}_3 + \tilde{d}_4(\tilde{\lambda}_4 - \tilde{u}_s)^2\tilde{\beta}_4 + \tilde{d}_5(\tilde{\lambda}_5 - \tilde{u}_s)^2\tilde{\beta}_5 \tag{A.6e}$$

for $\tilde{\beta}_k$. Here,

$$\tilde{r}_2 = \tilde{\epsilon}_s \Delta p_g, \quad \tilde{r}_4 = -\frac{\tilde{\epsilon}_s}{\rho_s}\Delta p_g, \quad \tilde{r}_5^S = -\frac{2}{3}\tilde{\epsilon}_s\tilde{T}_s\Delta u_s \quad \text{and} \quad \tilde{r}_5^P = \frac{2}{3}\tilde{u}_s\Delta(\epsilon_s T_s)$$

for Model A and

$$\tilde{r}_2 = 0, \quad \tilde{r}_4 = 0, \quad \tilde{r}_5^S = -\frac{2}{3}\tilde{\epsilon}_s\tilde{T}_s\Delta u_s \quad \text{and} \quad \tilde{r}_5^P = \frac{2}{3}\tilde{u}_s\Delta(\epsilon_s T_s)$$

for Model B. As with the wave strengths, algebraic expressions of $\tilde{\beta}_{1,2}$ are complicated. Thus, we solve (A.6c), (A.6d) and (A.6e) to obtain $\tilde{\beta}_{3,4,5}$,

$$\tilde{\beta}_k = \frac{(2\tilde{u}_s - \tilde{\lambda}_a - \tilde{\lambda}_b)\tilde{r}_4 + \tilde{r}_5}{\tilde{d}_k(\tilde{\lambda}_k - \tilde{\lambda}_a)(\tilde{\lambda}_k - \tilde{\lambda}_b)}$$

where $k \neq a \neq b$, and then solve $\tilde{\beta}_{1,2}$ in terms of the other values of $\tilde{\beta}$,

$$\tilde{\beta}_{1,2} = \mp \frac{\tilde{\lambda}_3\tilde{\beta}_3 + \tilde{\lambda}_4\tilde{\beta}_4 + \tilde{\lambda}_5\tilde{\beta}_5 - (\tilde{\beta}_3 + \tilde{\beta}_4 + \tilde{\beta}_5)\tilde{\lambda}_{2,1} - \tilde{r}_2}{\tilde{\lambda}_1 - \tilde{\lambda}_2}.$$

B C-Property Proof

To demonstrate that the numerical scheme satisfies the C-property, we apply the following basic steady state solution to the numerical scheme,

$$\rho_g = R, \quad u_g = u_s = 0, \quad \epsilon_s = G(x) \quad \text{and} \quad T_s = \frac{P_s}{\epsilon_s}.$$

For this steady state solution, the discharges and pressures are constant. The two velocities must be equal since, in the presence of the drag force, the two velocities tend to equality if no boundary conditions are prescribed. Thus, the above steady state solution is the only viable test case without applying boundary conditions.

When we apply this steady state solution to the numerical scheme, the eigenvalues become,

$$\tilde{\lambda}_{1,2} = \mp \tilde{c}_g \sqrt{\tilde{\epsilon}_g^{-1}}, \quad \tilde{\lambda}_3 = 0, \quad \tilde{\lambda}^S_{4,5} = \mp \sqrt{\tilde{T}_s} \quad \text{and} \quad \tilde{\lambda}^P_{4,5} = \mp \frac{1}{3}\sqrt{15\tilde{T}_s},$$

with corresponding eigenvectors

$$\tilde{\mathbf{e}}_{1,2} = \begin{bmatrix} 1 \\ \tilde{\lambda}_{1,2} \\ 0 \\ 0 \\ 0 \end{bmatrix}, \quad \tilde{\mathbf{e}}_3 = \begin{bmatrix} 1 \\ 0 \\ \tilde{d}_3 \\ 0 \\ 0 \end{bmatrix} \quad \text{and} \quad \tilde{\mathbf{e}}_k^{4,5} = \begin{bmatrix} 1 \\ \tilde{\lambda}_k \\ \tilde{d}_k \\ \tilde{\lambda}_k \tilde{d}_k \\ \tilde{d}_k(\tilde{\lambda}_{4,5} - \tilde{u}_s)^2 \end{bmatrix}.$$

Since the pressures are constant, the wave strengths simplify to

$$\tilde{\alpha}_{1,2} = \frac{1}{2}(\Delta(\epsilon_g \rho_g) - \tilde{\alpha}_3), \quad \tilde{\alpha}_3 = \frac{R\tilde{\epsilon}_s \Delta T_s}{\tilde{T}_s} \quad \text{and} \quad \tilde{\alpha}_{4,5} = 0$$

and the inhomogeneous terms are all zero, i.e. $\tilde{\beta}_k = 0$.

We can simplify $\tilde{\alpha}_{1,2}$ even further to

$$\tilde{\alpha}_{1,2} = -\frac{R}{2\tilde{T}_s}\left(\tilde{T}_s \Delta \epsilon_s + \tilde{\epsilon}_s \Delta T_s\right) = -\frac{R}{2\tilde{T}_s}\Delta(\epsilon_s T_s) = 0.$$

Thus, since $\tilde{\alpha}_k |\tilde{\lambda}_k| = 0$ for all k, the numerical flux-function becomes

$$\mathbf{F}^*_{i+\frac{1}{2}} = \begin{bmatrix} 0 \\ p_g \\ 0 \\ L \\ 0 \end{bmatrix} \quad \Rightarrow \quad \mathbf{F}^*_{i+\frac{1}{2}} - \mathbf{F}^*_{i-\frac{1}{2}} = 0.$$

Hence, the scheme is exact when applied to this steady state solution and thus, satisfies the C-property.

C The Gas Energy Equation

For non-isentropic flow, the gas Energy equation

$$(\epsilon_g E_g)_t + (\epsilon_g u_g (E_g + p_g))_x + p_g(\epsilon_g)_t = -\beta u_g (u_g - u_s)$$

can be appended to Model A and

$$(\epsilon_g E_g)_t + (u_g(\epsilon_g E_g + p_g))_x = -\beta u_g (u_g - u_s)$$

to Model B, where the total energy per unit volume is

$$E_g = \left(e_g + \frac{1}{2} u_g^2 \right) \rho_g$$

and the specific internal energy (for ideal gases) is

$$e_g = \frac{p_g}{(\gamma_g - 1)\rho_g} \quad \Rightarrow \quad p_g = (\gamma_g - 1)(E_g - \frac{1}{2}\rho_g u_g^2).$$

For further discussion on the presence of the time derivative $(\epsilon_g)_t$, see Gidaspow [10].

References

[1] A. Bermúdez & M. E. Vázquez, Upwind Methods for Hyperbolic Conservation Laws with Source Terms, *Computers and Fluids* **Vol. 23 No. 8**, 1049 - 1071 (1994).

[2] A. Boemer, H. Qi & U. Renz, Eulerian Simulation of Bubble Formation at a Jet in a Two-Dimensional Fluidized Bed, *Int. J. Multiphase Flow* **Vol. 23 No. 5**, 927 - 944 (1997).

[3] J.X. Bouillard, R.W. Lyczkowski & D. Gidaspow, Porosity Distributions in a Fluidized Bed with an Immersed Obstacle, *AIChE J.* **35**, 908 - 992 (1989).

[4] J. Ding & D. Gidaspow, A Bubbling Fluidization Model Using Kinetic Theory of Granular Flow, *AIChE J.* **Vol. 36 No. 4**, 523 - 538 (1990).

[5] D.A. Drew, Mathematical Modelling of Two-Phase Flow, *Ann. Rev. Fluid Mech.* **15**, 261 - 291 (1983).

[6] B. Eindfelt, C.D. Munz, P.L. Roe & B. Sjogreen, On Godunov-Type Methods Near Low Densities, *J. Comput. Phys.* **92**, 273 - 292 (1991).

[7] Li. Gascon & J.M. Corberan, Construction of Second-Order TVD Schemes for Nonhomogeneous Hyperbolic Conservation Laws, *J. Comput. Phys.* **172**, 261 - 297 (2001).

[8] D. Gidaspow, Hydrodynamics of Fluidization and Heat Transfer : Supercomputer Modelling, *Appl. Mech. Rev.* **39**(1), 1 - 23 (1986).

[9] D. Gidaspow, R. Bezburuah & J. Ding, Hydrodynamics of Circulating Fluidized Beds; Kinetic Theory Approach, *Fluidization VII, Proceedings of the 7th Engineering Foundation Conference on Fluidization*, 75 - 82 (1992).

[10] D. Gidaspow, *Multiphase Flow and Fluidization*, Academic Press, ISBN 0122824709 (1994).

[11] A. Harten, High Resolution Schemes for Conservation Laws, *J. Comput. Phys.* **49**, 357 - 393 (1983).

[12] M.E. Hubbard & P. Garcia-Navarro, Flux Difference Splitting and the Balancing of Source Terms and Flux Gradients, *J. Comput. Phys.* **165**, 89 - 125 (2000).

[13] N. Huber & M. Sommerfeld, Modelling and Numeric Calculation of Dilute-Phase Pneumatic Conveying in Pipe Systems, *Powder Technology* **99**, 90 - 101 (1998).

[14] J. Hudson, Numerical Techniques for Morphodynamic Modelling, PhD Thesis, *University of Reading*, October 2001. A colour postscript version of this thesis can be obtained at www.rdg.ac.uk/maths.

[15] R. Jackson, The Mechanics of Fluidized Beds. I: the Stability of the State of Uniform Fluidization, *Trans. Inst. Chem. Eng.* **41**, 13 - 21 (1963).

[16] R. Jackson, Locally Averaged Equations of Motion for a Mixture of Identical Spherical Particles and a Newtonian Fluid, *Chem. Eng. Sci.* **52**, 2457 - 2469 (1997).

[17] R. Jackson, *The Dynamics of Fluidized Particles*, Cambridge Monographs on Mechanics, ISBN 0-521-78122-1 (2000).

[18] J.T. Jenkins & S.B. Savage, A Theory for the Rapid Flow of Identical, Smooth, Nearley Elastic Spherical Particles, *J. Fluid Mech.* **130**, 187 - 202 (1983).

[19] G.E. Klinzing, R.D. Marcus, F. Rizk & L.S. Leung, *Pneumatic Conveying of Solids: A Theoretical and Practical Approach*, Powder Technology Series, Chapman and Hall, ISBN 0 412 72440 5 (1997).

[20] R.J. LeVeque, Balancing Source Terms and Flux Gradients in High-Resolution Godunov Methods: The Quasi-Steady Wave Propagation Algorithm, *J. Comput. Phys.* **146**, 346 - 365 (1998).

[21] R. J. LeVeque, *Finite Volume Methods for Hyperbolic Problems*, Cambridge Tezts In Applied Mathematics, ISBN 0 521 00924 3 (2002).

[22] R.J. LeVeque & H.C. Yee, A Study of Numerical Methods for Hyperbolic Conservation Laws with Stiff Source Terms, *J. Comput. Phys.* **86**, 187 - 210 (1990).

[23] C.K.K. Lun, S.B. Savage, D.J. Jeffrey & N. Chepurnity, Kinetic Theories for Granular Flow: Inelastic Particles in Couette Flow and Slightly Inelastic Particles in a General Flowfield, *J. Fluid Mech.* **140**, 223 - 256 (1983).

[24] R.W. Lyczkowski, Transient Propagation Behavior of Two-Phase Flow Equations, *AIChE Symp. Ser.* **75** (174), 165 - 174 (1978).

[25] R.W. Lyczkowski, D. Gidaspow, C.W. Solbrig & E.D. Hughes, Characteristics and Stablility Analyses of Transient One-Dimensional Two-Phase Flow Equations and Their Finite Difference Approximations, *Nucl. Sci. and Eng.* **66**, 378 - 396 (1978).

[26] P.L. Roe, Approximate Riemann Solvers, Parameter Vectors and Difference Schemes, *J. Comput. Phys.* **43**, 357 - 372 (1981).

[27] P.L. Roe, Some Contributions to the Modelling of Discontinuous Flows, *Lecture Notes Appl. Math.* **22**, 163 - 193 (1985).

[28] G. Rudinger & A. Chang, Analysis of Non-Steady Two-Phase Flow, *Physics of Fluids* **7**, 1747 - 1754 (1964).

[29] S.B. Savage & D.J. Jeffrey, The Stress Tensor in a Granular Flow at High Shear Stress, *J. Fluid Mech.* **110**, 255 (1981).

[30] H.B. Stewart & B. Wendroff, Two-Phase Flows: Models and Methods, *J. Comput. Phys.* **56**, 363 - 409 (1984).

[31] P.K. Sweby, High Resolution Schemes Using Flux Limiters for Hyperbolic Conservation Laws, *SIAM J. Num. Anal.* **21**, 995 (1984).

[32] M. Syamlal, W. Rogers & T.J. O'Brian, MFIX Documentation, Theory Guide, *Technical Note* DOE/METC-94/1004 (1993).

[33] B. van Leer, Towards the ultimate conservative difference scheme II. Monotonicity and conservation combined in a second order scheme, *J. Comput. phys.* **14**, 361 - 370 (1974).